Fabrication and Characterization of Hematite/Titanium Dioxide Photocatalyst for Hydrogen Production

Weerapong Bootluck

A Thesis Submitted in Fulfillment of the Requirements for the Degree of Doctor of Philosophy in Sustainable Energy Management

Prince of Songkla University

2022

Fabrication and Characterization of Hematite/Titanium Dioxide Photocatalyst for Hydrogen Production

Weerapong Bootluck

A Thesis Submitted in Fulfillment of the Requirements for the Degree of Doctor of Philosophy in Sustainable Energy Management

Prince of Songkla University

2022

Thesis Title Fabrication and Characterization of Hematite/Titanium Dioxide Photocatalyst for Hydrogen Production

Author Mr. Weerapong Bootluck

Major Program Sustainable Energy Management

Major Advisor

.....

(Asst. Prof. Dr. Watsa Khongnakorn)

Co-advisor

.....

(Assoc. Prof. Dr. Thawat Chittrakarn)

Examining Committee :

.....Chairperson

(Assoc. Prof. Dr. Apiluck Eaid-uae)

.....Committee

(Assoc. Prof. Dr. Warangkana Jutidamrongphan)

.....Committee

(Assoc. Prof. Dr. Kuaanan Techato)

.....

(Assoc. Prof. Dr. Thawat Chittrakarn)

.....

(Asst. Prof. Dr. Watsa Khongnakorn)

The Graduate School, Prince of Songkla University, has approved this thesis as fulfillment of the requirements for the Doctor of Philosophy Degree in Sustainable Energy Management

.....

(Prof. Dr. Damrongsak Faroongsarng)

Dean of Graduate School

This is to certify that the work here submitted is the result of the candidate's own investigations. Due acknowledgement has been made of any assistance received.

.....Signature
(Asst. Prof. Dr. Watsa Khongnakorn)
Major Advisor

.....Signature
(Assoc. Prof. Dr. Thawat Chittrakarn)
Co-advisor

.....Signature
(Mr. Weerapong Bootluck)
Candidate

I hereby certify that this work has not been accepted in substance for any degree, and is not being currently submitted in candidature for any degree.

.....Signature

(Mr. Weerapong Bootluck)

Candidate

ชื่อวิทยานิพนธ์ การสังเคราะห์และศึกษาคุณสมบัติตัวเร่งปฏิกิริยาเชิงแสงชนิดเฮมาไทต์/ไทเทเนียมไดออกไซด์สำหรับผลิตไฮโดรเจน

ผู้เขียน นายวีรพงค์ บุตรลักษณ์

สาขา การจัดการพลังงานอย่างยั่งยืน

ปีการศึกษา 2564

บทคัดย่อ

การศึกษานี้มีวัตถุประสงค์เพื่อพัฒนาตัวเร่งปฏิกิริยาเชิงแสงเพื่อใช้สำหรับผลิตแก๊สไฮโดรเจน โดยใช้วัสดุผสมชนิดไทเทเนียมไดออกไซด์กับเฮมาไทต์ ร่วมกับแพลลาเดียม และการปรับปรุงผิวด้วยเทคนิคพลาสมา ผลจากการศึกษาการปรับปรุงตัวเร่งปฏิกิริยาเชิงแสงชนิด α-Fe_2O_3/TiO_2-Pd พบว่าลักษณะโครงสร้างสันฐานวิทยามีขนาดโครงสร้างผลึกเฉลี่ยเท่ากับ 22 นาโนเมตร และมีแถบช่องว่างพลังงานเท่ากับ 2.00 อิเล็กตรอนโวล โดยแถบช่องว่างพลังงานน้อยกว่าชนิดไททาเนียมไดออกไซด์บริสุทธิ์ (3.16 อิเล็กตรอนโวลต์) ขนาดพื้นที่ผิวของตัวเร่งปฏิกิริยาเพิ่มขึ้นและมีรัศมีความต้านทาน EIS น้อยส่งผลทำให้เกิดการเคลื่อนที่ระหว่างประจุได้ดี โดยตัวเร่งปฏิกิริยาเชิงแสงชนิด α-Fe_2O_3/TiO_2-Pd มีประสิทธิภาพในการผลิตไฮโดรเจนได้ดีที่สุด เท่ากับ 3490.54 มิลลิโมลต่อชั่วโมง และให้ประสิทธิภาพในการนำกลับมาใช้ซ้ำในการเร่งปฏิกิริยาเชิงแสงสำหรับผลิตไฮโดรเจนได้เป็นอย่างดี

การศึกษาการปรับปรุงผิวตัวเร่งปฏิกิริยาเชิงแสงชนิด α-Fe_2O_3/TiO_2 ด้วยเทคนิคพลาสมา จากการศึกษาพบว่าลักษณะโครงสร้างสันฐานวิทยา พบว่าตัวเร่งปฏิกิริยาชนิด α-Fe_2O_3/TiO_2-10 มีความเหมาะสมที่สุด โดยผลจากการศึกษาโครงสร้างผลึกไททาเนียมไดออกไซด์โครงสร้างผลึกเปลี่ยนเป็นโครงสร้างผลึกผสมแบบอะนาเทสและแบบรูไทล์ โดยมีขนาดอนุภาคโครงสร้างผลึกเฉลี่ยลดลงจาก 25 ถึง 20 นาโนเมตร แถบช่องว่างพลังงานลดลงจาก 2.18 ถึง 1.84 อิเล็กตรอนโวลต์ และสามารถดูดกลืนแสงในช่วงวิสิเบิล (ช่วงความยาวคลื่น 400-700 นาโนเมตร) จากนั้นศึกษาความต้านทานทางไฟฟ้าเคมีพบว่าลดลงจาก 2.24 ถึง 1.90 กิโลโอห์ม การปรับปรุงผิวด้วยอาร์กอนพลาสมายังส่งผลให้เกิดช่องว่างของออกซิเจนและTi^{3+} ซึ่งส่งผลให้ประสิทธิภาพการเร่งปฏิกิริยาเชิงแสงสำหรับผลิตไฮโดรเจนภายใต้ช่วงแสงวิสิเบิลได้ดี เมื่อนำตัวเร่งปฏิกิริยาเชิงแสงนำไปทดสอบการแยกแก๊สไฮโดรเจนในช่วงแสงวิสิเบิล พบว่าตัวเร่งปฏิกิริยาเชิงแสงชนิด α-Fe_2O_3/TiO_2-10 สามารถผลิตแก๊สไฮโดรเจนดีที่สุดเท่ากับ 1.25 มิลลิโมลต่อชั่วโมง

คำนำ : โฟแตแคตะลิส เฮมาไทต์ ไทเทเนียมไดออกไซด์ ไฮโดรเจน

Thesis Title Fabrication and Characterization of Hematite/Titanium Dioxide Photocatalyst for Hydrogen Production

Author Mr. Weerapong Bootluck

Major Program Sustainable Energy Management

Academic Year 2021

ABSTRACT

This research aims to the development of photocatalytic α-Fe_2O_3/TiO_2 for hydrogen production by using noble metal deposition and plasma treatment. This study was to modification of heterojunctions of hematite (α-Fe_2O_3) deposition on titanium dioxide (TiO_2) and Palladium (Pd) co-catalyst. As the result of the characterization, the average crystallite size of ternary α-Fe_2O_3/TiO_2-Pd was 22 nm and its band gap energy was 2.00 eV, much lower than that of the pure TiO_2 nanoparticles (3.16 eV). The α-Fe_2O_3/TiO_2-Pd also has higher specific surface area and smaller EIS radius, which enhance interface activity and charge transfer. The α-Fe_2O_3/TiO_2-Pd exhibited great performance, with H_2 production rate of 3490.54 μmol h^{-1} g^{-1} and excellent stability in multi-cycle H_2 production.

Plasma modification on α-Fe_2O_3/TiO_2 photocatalyst, the crystalline phase of TiO_2 form changed from pure anatase to a mixture of anatase and rutile phases. The particle size was reduced from 25 to 20 nm. The band gap energy decreased from approximately 2.18 eV to 1.84 eV and exhibited a wider absorption edge under visible light irradiation (400–700 nm). The charge transfer resistance was reduced from 2.24 to 1.90 kΩ. Ar-plasma modification of the surface showed the attribution of oxygen vacancies and Ti^{3+}. The plasma treatment improved the heterojunction photocatalyst to enhance the photocatalytic activity under visible light for H_2 evolution. The best photocatalytic activity for H_2 evolution rate was obtained at 1.25 mmol h^{-1} for α-Fe_2O_3/TiO_2-10 photocatalyst

Keyword : Photocatalyst, Hematite, Titanium Dioxide, Hydrogen

ACKNOWLEDGEMENT

I would like to thank my advisor, Asst. Prof. Dr. Watsa Khongnakorn. I would like to thank for her invaluable suggestion and lessons for my academic knowledge, guidance, kindness and assistant during my study. I would like to thank my co-advisor, Assoc. Prof. Dr. Thawat Chittrakarn. I also would like to thank you for your guidance during my study.

I would like to thank Asso. Prof. Dr. Kuuanan Techato, Asso. Prof. Dr. Apiluck Eiad-ua and Asso. Prof. Dr. Warangkana Jutidamrongphan for guidance and suggestions during this work.

I am also grateful to Faculty of Environmental Management, Prince of Songkla University, Center of Excellence in Membrane Science and Technology, PSU Energy Systems Research Institute and graduate school, Prince of Songkla University for financial support.

I would like to thank my family and Miss. Warunee Saelee for their support during my study.

Weerapong Bootluck

CONTENTS

Page

LIST OF TABLES

Page

LIST OF FIGURES

Page

LIST OF FIGURES (CONTINUED)

Page

LIST OF FIGURES (CONTINUED)

Page

LIST OF ABBREVIATION

A	Constant
α	The absorbance
Ag/AgCl	Reference Electrode
AFM	Atomic force microscopy
Ar	Argon
β	The peak width at half maximum (FWHM) of the XRD peak
Cu_2O	Copper (I) oxide
$CoFe_2O_4$	Cobalt ferrite
d	The crystallite size (nm)
θ	The diffraction angle
Eg	Band gap energy
EIS	Electrochemical impedance
EtOH	Ethanol
$Fe(NO_3)_3.9H_2O$	Iron(III) nitrate nonahydrate
FTO	Fluorine-doped tin oxide
Hz	Hertz
ICP-OES	Inductively coupled plasma optical emission spectrometer
k	Constant related to the crystallite shape normally taken as 0.89
α-Fe_2O_3	Hematite
GC	Gas chromatography
GO	Graphite oxide
g-C_3N_4	Graphitic carbon nitrides
h	Planck's constant
λ	The X-ray wavelength (nm)
mV	Millivolts
nm	Nanometer
Na_2SO_4	Sodium sulfate

LIST OF ABBREVIATION (CONTINUED)

Pd	Palladium
PL	Photoluminescence spectroscopy
Pt	Platinum
UV-Vis	UV–vis spectrometry
SEM	Scanning electron microscopy
TCD	Thermal conductivity detector
Ti $(OC(CH_3)_3)_4$	Titanium (IV) butoxide
Ti	Titanium foil
TiO_2	Titanium dioxide
TEM	Transmission electron microscopy
XPS	X-ray photoelectron spectroscopy
SnO_2	Tin (IV) oxide
ν	The light frequency
W	Watts
WO_3	Tungsten trioxide
XRD	X-ray Diffractometry
ZnO	Zinc Oxide

LIST OF PAPERS

I. Bootluck, W., Chittrakarn, T., Techato, K., Jutaporn, P and Khongnakorn, W. 2021. S-Scheme α-Fe_2O_3/TiO_2 Photocatalyst with Pd Cocatalyst for Enhanced Photocatalytic H_2 Production Activity and Stability. Catalysis Letters. 1-17.

II. Bootluck, W., Chittrakarn, T., Techato, K and Khongnakorn, W. 2021. Modification of surface α-Fe_2O_3/TiO_2 photocatalyst nanocomposite with enhanced photocatalytic activity by Ar gas plasma treatment for hydrogen evolution. Journal of Environmental Chemical Engineering, 9 (4), 105660.

PAPER I

Reprint was made permission from the publisher

SPRINGER NATURE LICENSE
TERMS AND CONDITIONS

Mar 16, 2022

This Agreement between Prince of Songkla University -- Weerapong Bootluck ("You") and Springer Nature ("Springer Nature") consists of your license details and the terms and conditions provided by Springer Nature and Copyright Clearance Center.

License Number	5270691427954
License date	Mar 16, 2022
Licensed Content Publisher	Springer Nature
Licensed Content Publication	Catalysis Letters
Licensed Content Title	S-Scheme α-Fe2O3/TiO2 Photocatalyst with Pd Cocatalyst for Enhanced Photocatalytic H2 Production Activity and Stability
Licensed Content Author	Weerapong Bootluck et al
Licensed Content Date	Dec 1, 2021
Type of Use	Thesis/Dissertation
Requestor type	academic/university or research institute
Format	print and electronic
Portion	full article/chapter
Will you be translating?	no
Circulation/distribution	5000 - 9999
Author of this Springer Nature content	yes
Title	Fabrication and Characterization of Hematite/Titanium Dioxide Photocatalyst for Hydrogen Production
Institution name	Prince of Songkla University
Expected presentation date	Mar 2022
Order reference number	0
Requestor Location	Prince of Songkla University Faculty of Environmental Management, Pri Hat Yai, Songkhla 90110 Thailand Attn: Prince of Songkla University
Total	**0.00 USD**
Terms and Conditions	

PAPER II

Reprint was made permission from the publisher

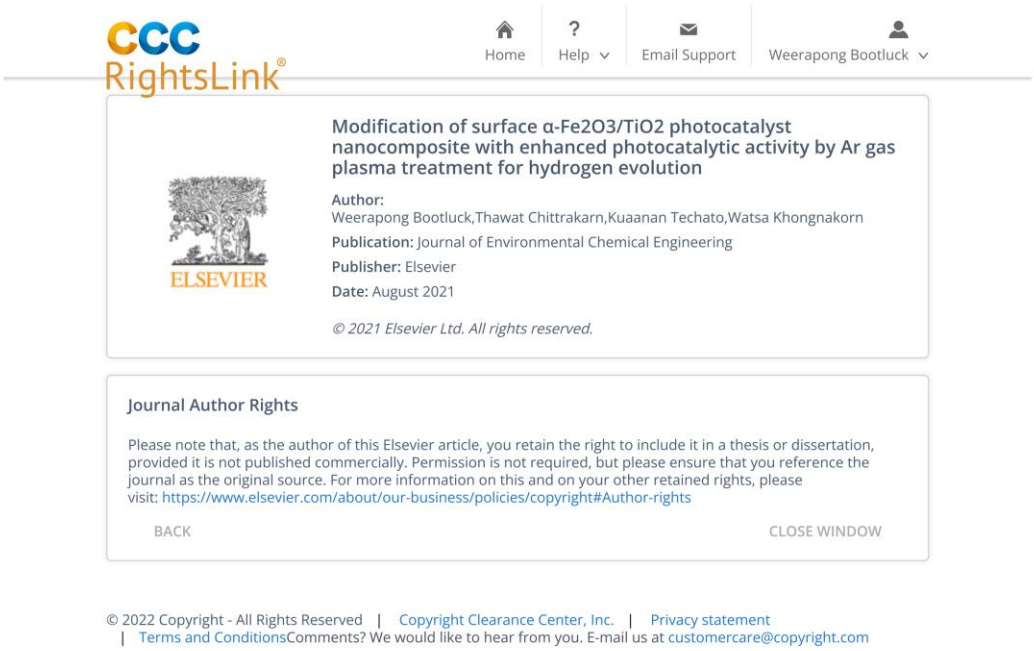

CCC RightsLink

Home | Help | Email Support | Weerapong Bootluck

Modification of surface α-Fe2O3/TiO2 photocatalyst nanocomposite with enhanced photocatalytic activity by Ar gas plasma treatment for hydrogen evolution

Author:
Weerapong Bootluck,Thawat Chittrakarn,Kuaanan Techato,Watsa Khongnakorn

Publication: Journal of Environmental Chemical Engineering

Publisher: Elsevier

Date: August 2021

© 2021 Elsevier Ltd. All rights reserved.

Journal Author Rights

Please note that, as the author of this Elsevier article, you retain the right to include it in a thesis or dissertation, provided it is not published commercially. Permission is not required, but please ensure that you reference the journal as the original source. For more information on this and on your other retained rights, please visit: https://www.elsevier.com/about/our-business/policies/copyright#Author-rights

BACK CLOSE WINDOW

CHAPTER 1
INTRODUCTION

1.1 Background

The energy crisis of the fossil fuel shortage and the increase of pollutant is the main issues of global concern. Nowadays, fossil fuels are increasing in energy demand [1,2]. Hydrogen (H_2) is considered one of the most promising renewable energy for sustainable energy and the environment. H_2 is an energy-efficient, non-pollutant and clean energy (H_2 burned only by-product is water) [3] Hydrogen production from solar light includes photoelectrochemical, photobiological and photocatalytic, the method is low cost and environmental friendly [4,5].

Photocatalytic water splitting for hydrogen production is one of the most methods to produce H_2 from solar, photocatalytic methods is a promising technology for H_2 evolution and separation that provides an application in H_2 evolution and wastewater treatment[6]. A semiconductor is a catalytic material that activity with a photon for hydrogen evolution and degradation of pollutants. Among semiconductor materials that have been used for photocatalytic efficiencies such as cadmium sulfide (CdS) [7], Zinc oxide (ZnO)[8], tungsten trioxide (WO_3) [9] and titanium dioxide (TiO_2) [10]. TiO_2 is the most widely used semiconductor material based for the photocatalytic process. It is used for a semiconductor in photocatalytic due to chemical stability, high reusability, low cost and excellent photocatalytic activity which include wide band gap energy (3.2 eV) [10]. Because of the wide bandgap energy of TiO_2 is absorption from the visible light which activity of photocatalytic. However, TiO_2 is limited for absorption from the solar region (visible light of 43 %) because of the pure TiO_2 absorption only of UV light radiation about 4 % of the total light [10,11]. The methods to modify the surface of semiconductor material are a key factor for photocatalytic efficiency. Numerous methods have been modifying photocatalytic material such as noble metal doping, metal doping [12], ion-doping [13] and modification surface [10]. Hematite (α-Fe_2O_3) is a noble metal oxide, with wider absorption visible light (400-700 nm) and low band gap energy (2.0-2.3 eV), due to its excellent nontoxic and is cost-effective [10].

The noble metal deposition of α-Fe_2O_3 on the TiO_2 can improve to wider absorption under visible light. Moreover, the deposition of ternary on the heterojunction can be improved photocatalytic activity, trapping the recombination electron-hole pair. The enhanced efficiency of photocatalytic activity has been reported deposition on heterojunction photocatalyst by platinum (Pt), silver (Ag) and palladium (Pd) etc. Palladium (Pd) is one of the noble metals due to its chemical properties are similar to platinum (Pt), high surface area, and great electron transfer chemical stability [11]. For the modification surface, the plasma treatment is a method for modifying the surface by etching of surface which changes the surface properties to enhanced photocatalytic activity. In addition, these methods of modifying to generating of oxygen vacancy and highly stable of Ti^{3+} on the surface of TiO_2, the increasing of the surface area including absorption under visible light and UV radiation and improve photogeneration of charge carrier [10].

This research aimed to improve the photocatalytic material of heterojunction of α-Fe_2O_3/TiO_2 with the ternary of Pd nanoparticle, and modification of the surface by plasma treatment for obtain for improve photocatalytic activity for hydrogen production under solar light and visible light. The photocatalytic membrane was to modify by plasma for H_2 production. The characterization of material in the surface morphology, chemical crystallite size, charge carrier separation, charge transfer, particle size, optical bandgap energy, elemental composition and chemical state, respectively. Finally, the photocatalytic material was investigated for H_2 production, stability and investigated in H_2 production.

1.2 The objective of this research was as follows

- To synthesis of the heterojunction hematite (α-Fe_2O_3) on titanium dioxide (TiO_2) photocatalytic and cocatalyst with palladium (Pd)
- To modified of photocatalytic hematite (α-Fe_2O_3) on titanium dioxide (TiO_2) photocatalytic by plasma treatment for hydrogen evolution

REFERENCE

[1] I. Dincer, C. Acar, Review and evaluation of hydrogen production methods for better sustainability, Int. J. Hydrogen Energy. 40 (2014) 11094–11111. https://doi.org/10.1016/j.ijhydene.2014.12.035.

[2] J.O. Abe, A.P.I. Popoola, E. Ajenifuja, O.M. Popoola, Hydrogen energy, economy and storage: Review and recommendation, Int. J. Hydrogen Energy. 44 (2019) 15072–15086. https://doi.org/10.1016/j.ijhydene.2019.04.068.

[3] N.L. Reddy, V.N. Rao, M. Vijayakumar, R. Santhosh, S. Anandan, M. Karthik, M. V. Shankar, K.R. Reddy, N.P. Shetti, M.N. Nadagouda, T.M. Aminabhavi, A review on frontiers in plasmonic nano-photocatalysts for hydrogen production, Int. J. Hydrogen Energy. 44 (2019) 10453–10472. https://doi.org/10.1016/j.ijhydene.2019.02.120.

[4] M. De Oliveira Melo, L.A. Silva, Visible light-induced hydrogen production from glycerol aqueous solution on hybrid Pt-CdS-TiO_2 photocatalysts, J. Photochem. Photobiol. A Chem. 226 (2011) 36–41. https://doi.org/10.1016/j.jphotochem.2011.10.012.

[5] C.W. Huang, C.H. Liao, J.C.S. Wu, Photocatalytic Separate Evolution of Hydrogen and Oxygen over Highly Ordered Nanorods and Bulk TiO_2 Thin Films, J. Clean Energy Technol. 1 (2013) 1–5. https://doi.org/10.7763/jocet.2013.v1.1.

[6] L. Yuan, C. Han, M.Q. Yang, Y.J. Xu, Photocatalytic water splitting for solar hydrogen generation: fundamentals and recent advancements, Int. Rev. Phys. Chem. 35 (2016) 1–36. https://doi.org/10.1080/0144235X.2015.1127027.

[7] T. Hu, K. Dai, J. Zhang, S. Chen, Noble-metal-free Ni_2P modified step-scheme $SnNb_2O_6$/CdS-diethylenetriamine for photocatalytic hydrogen production under broadband light irradiation, Appl. Catal. B Environ. 269 (2020) 118844. https://doi.org/10.1016/j.apcatb.2020.118844.

[8] C.V. Reddy, K.R. Reddy, N.P. Shetti, J. Shim, T.M. Aminabhavi, D.D. Dionysiou, Hetero-nanostructured metal oxide-based hybrid photocatalysts for enhanced photoelectrochemical water splitting – A review, Int. J. Hydrogen Energy. (2019). https://doi.org/10.1016/j.ijhydene.2019.02.109.

[9] J. Fu, Q. Xu, J. Low, C. Jiang, J. Yu, Ultrathin 2D/2D WO_3/g-C_3N_4 step-

scheme H_2-production photocatalyst, Appl. Catal. B Environ. 243 (2019) 556–565. https://doi.org/10.1016/j.apcatb.2018.11.011.

[10] W. Bootluck, T. Chittrakarn, K. Techato, W. Khongnakorn, Modification of surface α-Fe_2O_3/TiO_2 photocatalyst nanocomposite with enhanced photocatalytic activity by Ar gas plasma treatment for hydrogen evolution, J. Environ. Chem. Eng. 9 (2021) 105660. https://doi.org/10.1016/j.jece.2021.105660.

[11] W. Bootluck, T. Chittrakarn, K. Techato, P. Jutaporn, W. Khongnakorn, S-Scheme α-Fe_2O_3/TiO_2 Photocatalyst with Pd Cocatalyst for Enhanced Photocatalytic H_2 Production Activity and Stability, Catal. Letters. (2021). https://doi.org/10.1007/s10562-021-03873-5.

[12] T. Jafari, E. Moharreri, A.S. Amin, R. Miao, W. Song, S.L. Suib, Photocatalytic water splitting - The untamed dream: A review of recent advances, Molecules. 21 (2016). https://doi.org/10.3390/molecules21070900.

[13] M. Asiltürk, F. Sayilkan, E. Arpaç, Effect of Fe^{3+} ion doping to TiO_2 on the photocatalytic degradation of Malachite Green dye under UV and vis-irradiation, J. Photochem. Photobiol. A Chem. 203 (2009) 64–71. https://doi.org/10.1016/j.jphotochem.2008.12.021.

CHAPTER 2

This study presents the development of heterojunction S-Scheme α-Fe_2O_3/TiO_2 photocatalyst with Pd cocatalyst for enhanced photocatalytic H_2 production activity and stability. The α-Fe_2O_3/TiO_2-Pd was obtained characterization by various techniques including XRD, UV-vis, FE-SEM, TEM, EDS and XPS, respectively. The migration of photogenerated charge carriers was performed by PL emission and transient photocurrent response. The ternary heterojunction of α-Fe_2O_3/TiO_2-Pd exhibits improve photocatalytic activity towards H_2 evolution rate and its stability under exposure to visible light is investigated. This article has been published in the title of "S-Scheme α-Fe $_2O_3/TiO_2$ Photocatalyst with Pd Cocatalyst for Enhanced Photocatalytic H_2 Production Activity and Stability in Catalysis Letters.

PAPER I

S-Scheme α-Fe_2O_3/TiO_2 Photocatalyst with Pd Cocatalyst for Enhanced Photocatalytic H_2 Production Activity and Stability.

Catalysis Letters. (2021) 1-17
https://doi.org/10.1007/s10562-021-03873-5

Catalysis Letters
https://doi.org/10.1007/s10562-021-03873-5

S-Scheme α-Fe_2O_3/TiO_2 Photocatalyst with Pd Cocatalyst for Enhanced Photocatalytic H_2 Production Activity and Stability

Weerapong Bootluck[1,2] · Thawat Chittrakarn[2] · Kuaanan Techato[1,3] · Panitan Jutaporn[4] · Watsa Khongnakorn[2,5]

Received: 25 April 2021 / Accepted: 19 November 2021

Abstract

In this work, hematite with titanium dioxide (α-Fe_2O_3/TiO_2) heterojunctions with palladium (Pd) nanoparticles were synthesised to improve efficiency of photocatalytic hydrogen production. α-Fe_2O_3 was loaded onto TiO_2 surfaces, then Pd nanoparticles were deposited to make a ternary photocatalyst. The chemical composition, morphology and surface properties of photocatalytic ternary heterojunction were characterized by XRD, UV–Vis, FE-SEM, TEM, EDS, XPS techniques and BET analysis. The PL emission, transient photocurrent and EIS Nyquist plot were investigated for separation and migration of photogenerated charge carriers in photocatalyst nanocomposites. The average crystallite size of ternary α-Fe_2O_3/TiO_2-Pd was 22 nm and its band gap energy was 2.00 eV, much lower than that of the pure TiO_2 nanoparticles (3.16 eV). The α-Fe_2O_3/TiO_2-Pd also has higher specific surface area and smaller EIS radius, which enhance interface activity and charge transfer. The α-Fe_2O_3/TiO_2-Pd exhibited great performance, with H_2 production rate of 3490.54 μmol h^{-1} g^{-1} and excellent stability in multi-cycle H_2 production. The photocatalytic mechanism of α-Fe_2O_3/TiO_2-Pd as explained by the S-scheme heterojunction is that the electron in the VB of α-Fe_2O_3 and TiO_2 are transferred to CB of each photocatalyst. Then, the electrons in the CB of TiO_2 are transferred to the VB of α-Fe_2O_3 and the photogenerated electrons in CB of α-Fe_2O_3 can migrate to Pd, which increase the redox ability for H_2 production and increase the separation of photogenerated e^-–h^+ pairs. Overall, the experimental results and theoretical analyses confirm the high potential for the applicability of the ternary photocatalysts for H_2 production.

Graphical Abstract

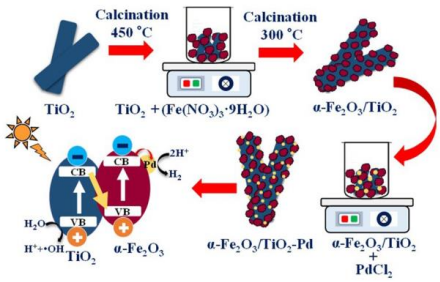

Keywords Photocatalysis · Heterojunction · α-Fe_2O_3/TiO_2-Pd · Hydrogen production · Pd-ternary

✉ Watsa Khongnakorn
watsa.k@psu.ac.th

Extended author information available on the last page of the article

Published online: 01 December 2021

1 Introduction

Developments in clean hydrogen power has risen rapidly during the last decade. The global hydrogen market is forecasted to increase to $155 billion in 2022, and the annual growth rate is higher than 6% [1]. Currently, industrial hydrogen production is mainly through steam reforming using fossil fuels and natural gas [2, 3]. However, fossil fuels use in hydrogen production is not considered sustainable for the future [4, 5]. Alternative renewable energy sources for hydrogen production include solar, wave, and biomass energies [6]. Solar energy could be converted to hydrogen through photoelectrolytic [7], photoelectrochemical [8, 9], photocatalytic [10], and photobiological methods [11]. Particularly, the photocatalytic approach is a promising technology as it is environment-friendly, technically feasible, and economically favourable [12], especially with photocatalytic water splitting [10, 12, 13]. Recent researches on photocatalytic water splitting has focused on improving hydrogen production rate and widening wavelength range of usable solar light [14, 15].

Several semiconductor materials, such as cadmium sulfide (CdS), zinc oxide (ZnO), tungsten trioxide (WO_3), bismuth vanadate ($BiVO_4$), iron (III) oxide (Fe_2O_3), molybdenum disulfide (MoS_2) graphitic carbon nitride (g-C_3N_4) nanocomposites [9, 10] and titanium dioxide (TiO_2) can be used as photocatalytic materials [14–16]. Among these, TiO_2 is often used in photocatalytic water splitting owing to its good reusability, chemical stability, economic feasibility, and low environmental impact [17, 18]. The key factors determining the performance of a photocatalyst include structure and morphology, crystallinity, band gap energy (E_g), and corrosion resistance. The high band gap energy of TiO_2 (3.2 eV) means it requires UV light to excite the electrons from valence band (VB) to the conduction band (CB), and UV radiation makes up just about 4% of the total energy in solar radiation [19, 20]. However, the efficiency of photocatalytic H_2 production over TiO_2 remains low because the photogenerated electrons in the CB quickly recombine with the holes (h^+) in the VB [21, 22]. Hence, to utilize the visible portion of sunlight (43%, $\lambda = 380–750$ nm), it is necessary to improve the band gap energy of TiO_2 [23, 24]. Many attempts have been made to hinder the e^-–h^+ recombination. For instance, methods such as doping, noble metal deposition, non-metal ions, and surface sensitization [9] have been used to modify photocatalytic TiO_2-based materials, to reduce the recombination of e^-–h^+ pairs and to advance the response of the photocatalyst to visible light [25, 26]. In photocatalytic heterojunctions, the direct contact of two semiconductors with suitable CB and VB potentials can provide charge transfer through the interface. Various types of heterojunctions formed in TiO_2-based composites have been shown to increase charge lifetime and enhance photocatalytic activity, such as WO_3/TiO_2, Cds/TiO_2, ZnO/TiO_2, Fe_2O_3/TiO_2, etc. [27, 28].

The Fe_2O_3/TiO_2 nanocomposite photocatalyst has been synthesized with heterojunction at the interface to improve photoactivity for the removal of pollutants from wastewater, and for water splitting in hydrogen production. Iron oxide (Fe_2O_3) is a metal oxide that can have various crystalline structures, such as magnetite (Fe_3O_4), maghemite (γ-Fe_2O_3), hematite (α-Fe_2O_3), etc. [29]. Hematite (α-Fe_2O_3) is the most stable form of iron oxides and it also has a narrow range of band gap energy of 2.0–2.3 eV [30–32]. Therefore, it can absorb light up to 600 nm and can also collect as much as 40% of the energy in solar radiation, based on the spectral energy distribution. Recently, α-Fe_2O_3 has been used as a photocatalytic material for hydrogen production via water splitting [33–35] due to its outstanding advantages, including low cost, chemical stability, and non-toxicity [19, 36]. However, Fe_2O_3 also suffers from a high e^-–h^+ recombination rate. Its poor conductivity means that an overpotential is needed to produce H_2. For example, Zhu et al. [37] and Huang et al. [38] developed two types of semiconducting heterojunctions of α-Fe_2O_3/TiO_2 to enhance photoactivity under visible light irradiation. Furthermore, Zhu et al. [37] has synthesized a hierarchical structure (H-Fe_2O_3/TiO_2), which showed higher efficiency in photocatalytic H_2 production under visible light. Madhumitha et al. [33] prepared α-Fe_2O_3/TiO_2 core–shell nanoparticle photocatalysts by co-precipitation and the obtained heterojunction could decrease charge transfer from TiO_2 to α-Fe_2O_3 by suppressing e^-–h^+ pair recombination.

On the other hand, noble metals deposition on semiconducting heterojunctions can improve the efficiency of photoelectron generation while inhibiting e^-–h^+ recombination, resulting in faster H_2 production. The enhanced efficiency with a ternary heterojunction photocatalyst at the interface of noble metal has been reported [27–29]. The ternary material nanocomposite was synthesized to eliminate the drawback of photocatalytic materials because the Schottky barrier formation and plasmonic Z-scheme at the heterojunction photocatalyst interface can prevent electron–hole recombination [27–29]. Güy et al. [16] introduced the ternary $MoS_2/Ag/Ag_3VO_4$ to delay recombination of photocarriers by plasmonic Z-scheme structure formation. Atacan et al. [8] prepared Ag_2CrO_4/GO/$MnFe_2O_4$ composite that was able to enhance H_2 production and increase electron density with Z-scheme structure. In addition, the step-scheme (S-scheme) heterojunction photocatalyst was divided into two types of semiconductor photocatalyst (p-type or n-type). S-scheme formed the photogenerated transfer of charge carriers and promoted the separation electron–hole pair. The internal electric

field is the main driving force of charge transfer between two semiconductor photocatalysts [39, 40]. Recently, the S-scheme ternary heterojunction has been reported [41, 42]. Zhu et al. [41] have studied the effectiveness of NiO as a co-catalyst of g-C_3N_4/TiO_2 on S-scheme photocatalyst heterojunction, which showed high-efficiency in the prevention of electrons and hole recombination. Hu et al. [42] developed a ternary S-scheme of Ni_2P and $SnNb_2O_6$/CdS-diethylenetriamine (SNO/CdS-D) to ease charge separation and high hydrogen harvesting. Yan et al. [43] studied the S-scheme ternary photocatalyst heterojunction of Co_3S_4/g–C_3N_4/α-Fe_2O_3. They showed high stable of hydrogen evolution due to high adsorption rate and high redox potential. Hence, the co-catalyst process is a promising technology to enhance photocatalyst properties. Palladium (Pd) is one of the noble metals that has been deposited on heterojunctions, and its chemical properties are similar to platinum (Pt). The advantages offered by Pd include low cost, stability, high surface area, and great electron transfer [44, 45]. The deposition of Pd nanoparticles can modify the photocatalytic surface and crystalline structure of the heterojunction and enhance the separation of e^-–h^+ pairs. The Pd co-catalyst could increase the photocatalytic hydrogen production rate by prolonging the lifetime of photogenerated e^-–h^+ pairs. In addition, Ramírez et al. [46], reported an increase in charge carriers with Pd nanoparticles deposited on WO_3–TiO_2 heterojunction. When Pt, Pd, and silver (Ag) were used as co-catalysts, Pd increased the photocatalytic activity and enabled strong recycling of the photocatalyzed reaction [47]. Chuaicham et al. [48] reported that the deposition of ternary Pd over sepiolight/g-C_3N_4 resulted in high efficiency of photocatalysis due to visible light absorption and prevention of e^-–h^+ recombination at the heterojunction of photocatalyst nanocomposite.

Given that deposition of Pd over WO_3–TiO_2 and sepiolight/g-C_3N_4 heterojunctions could increase the photocatalytic activity and prevent e^-–h^+ recombination, a ternary photocatalyst S-scheme of α-Fe_2O_3/TiO_2 with ternary Pd heterojunctions would be able to combine the advantages of this nanocomposite photocatalyst with an improvement in stability of H_2 production. Based on the literature review above, the performance of ternary Pd nanoparticles deposition on photocatalytic α-Fe_2O_3/TiO_2 heterojunction for H_2 generation have not been evaluated. Hence, in this study, ternary Pd is introduced into heterojunction photocatalyst nanocomposites, to form ternary heterojunction α-Fe_2O_3/TiO_2-Pd nanocomposites. These nanocomposites morphology and pore structure are characterized by various techniques include FE-SEM, TEM, EDS, XRD, UV–Vis, XPS, and BET respectively. The migration photogenerated of charge carriers was performed by PL emission, EIS and transient photocurrent response. The ternary heterojunction of α-Fe_2O_3/TiO_2-Pd exhibit improve photocatalytic activity towards H_2 evolution rate and its stability under exposure to visible light are investigated.

2 Materials and Methods

2.1 Materials

Titanium butoxide ($Ti(OC(CH_3)_3)_4$) and palladium chloride ($PdCl_2$) were obtained from Sigma-Aldrich. Ethylene glycol (EG) was purchased from Loba Chemie. Iron (III) nitrate nonahydrate ($Fe(NO_3)_3{\cdot}9H_2O$) was procured from Ajax Finechem. Ethanol and methanol (AR, 99.9%) were purchased from RCI Labscan.

2.2 Synthesis of TiO_2 Nanoparticles

TiO_2 was prepared using a method previously reported by Peng et al. [49] with slight modifications. First, 3 mL of titanium butoxide and 30 mL of ethylene glycol were added into a flask and heated at 180 °C for 2 h. After the solution was allowed to cool down to room temperature, the white precipitate products were centrifuged. The precipitates were then washed with ethanol several times, followed by drying at room temperature. Finally, the products were calcined at 450 °C for 2 h, then TiO_2 was obtained as dried powder.

2.3 Preparation of α-Fe_2O_3/TiO_2

To prepare α-Fe_2O_3/TiO_2, 1.5 g of TiO_2 powder was added in 30 mL ethanol with 50 wt% Fe $(NO_3)_3{\cdot}9H_2O$. The selected synthesis proportions, with 50 wt% loading of α-Fe_2O_3 on TiO_2 nanocomposite, gave the best photocatalytic activity as reported by Huang et al. [38]. The sample was stirred for 30 min and then evaporated at 50 °C. The photocatalytic Fe_2O_3/TiO_2 nanocomposite was then calcined at 300 °C for 10 min. Finally, the α-Fe_2O_3/TiO_2 nanocomposite was heated at 5 °C/min to reach 300 °C and calcined for 6 h and the product was labelled as α-Fe_2O_3/TiO_2.

2.4 Pd Deposition on α-Fe_2O_3/TiO_2 Nanoparticles

The α-Fe_2O_3/TiO_2 nanoparticles were dispersed in 50 mL deionized (DI) water. Then, $PdCl_2$ solution was dropped into the dispersion under magnetic stirring for a 1.0 wt% loading following a procedure reported by Chuaicham et al. [48], and irradiated under a 250 W Hg arc lamp for 1 h [50]. Afterwards, the sample was washed with ethanol several times and dried at 60 °C for 120 min. The prepared sample was labelled as α-Fe_2O_3/TiO_2-Pd. The preparation procedure is schematically shown in Fig. 1.

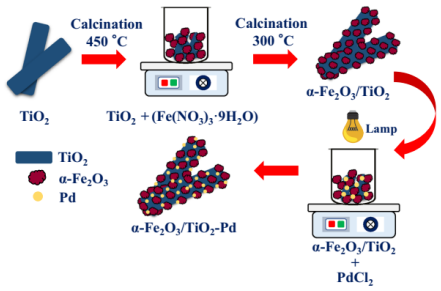

Fig. 1 Schematic illustration of the synthesis of α-Fe_2O_3/TiO_2-Pd photocatalytic heterojunction nanocomposite

2.5 Material Characterisation

Surface morphology of the synthesised α-Fe_2O_3/TiO_2-Pd nanocomposite were analysed using field-emission scanning electron microscopy (FESEM, Apreo, FEI, USA) and transmission electron microscopy (TEM; Tecnai G2 F20). The textural properties of the photocatalysts was analyzed for their porosity, specific surface area (SSA) and nitrogen (N_2) adsorption–desorption isotherm by Brunauer–Emmett–Teller (BET) analyzer (Micromeritics ASAP 2460,USA) [51]. Before BET analyses, the temperature was set at 190 °C for 3 h for degassing [52]. The pore size distribution was calculated from the desorption curve by BJH method. The average crystallite size was determined using an X-ray diffractometer (XRD; X'Pert MPD, PHILIPS, Netherlands) by scanning of 2θ range from 20° to 80°. The calculation of crystallite size and crystallinity followed Scherrer's equation [53]:

$$D = \frac{k\lambda}{\beta \mathrm{Cos}\theta} \tag{1}$$

where k is a shape factor constant (0.9), λ is the X-ray wavelength (nm), θ is the diffraction angle, D is the crystallite size (nm), and β is the full width at half maximum (FWHM) of the diffraction line. Electronic states of elements on the heterojunction surface were analysed by X-ray photoelectron spectroscopy (XPS; AXIS Ultra DLD, Krotos, UK). The band gap energy was calculated from the UV–Vis spectrum recorded with a UV-2401 instrument (Shimadzu, Japan). The recombination and separation efficiency of charge carriers was investigated with a photoluminescence spectrometer (PL; Avantes AvaSpec-2048, Netherlands). The transient photocurrent, electrochemical impedance spectroscopy (EIS) and Mott-Schottky measurements were conducted with a potentiostat (Potentiostat/Galvanostats PGSTAT302N Metrohm, Autolab, Netherland). The instrument configuration was set according to a protocol published previously [42–44] and the working electrode was prepared following Duo et al. [54].

The average crystallite size was calculated from the XRD peak using the Debye–Scherrer equation [53, 55]. The band gap energy near valence band of TiO_2 and α-Fe_2O_3 nanoparticles was calculated from the following Tac's plot equation [56, 57]:

$$\alpha h\nu = A(h\nu - E_g)^{n/2} \tag{2}$$

where α is an absorption coefficient, h is a Planck constant, ν is an incident light frequency, A is a constant, E_g is the band gap and n is an integer. The value of n depends on the type of optical transition and the value of 1 was selected for direct observed optical transition for all the samples [56]. The VB of TiO_2 and α-Fe_2O_3 was determined by using XPS spectra. The CB and band edge position were performed according to our previous study [57]. The work function of photocatalyst was calculated according to Ren et al. [58].

2.6 Photocatalytic Activity of H_2 Production

The photocatalytic reactor was set up with a plexiglas cell of 100 mL. A 300 W UV lamp and visible light mercury lamps (250 W, $\lambda \geq 420$ nm) were used as light sources. The α-Fe_2O_3/TiO_2-Pd photocatalyst (0.1 g) was added to 100 mL solution of a sacrificial agent (methanol: water = 30:70 v/v). Before the reaction, nitrogen gas was delivered into the reactor for 60 min [4]. The produced H_2 was analysed by gas chromatography (GC, Hewlett Packard, HP 6890, USA) with a thermal conductivity detector (TCD) and using helium as the carrier gas. The generated H_2 amount was calculated by Heider and Kang method [59]. For multi-cycle H_2 production, after 4-h cycle, the used catalyst was thoroughly cleaned and dried then reused again for the next cycle. The recycling stability of the sample was calculated following the protocol according to a previous study [60].

3 Results and Discussion

3.1 Characterisation of α-Fe_2O_3/TiO_2-Pd Photocatalytic Nanocomposites

The XRD patterns of different types of α-Fe_2O_3/TiO_2-Pd synthesized are shown in Fig. 2. There are five characteristic diffraction peaks of pure anatase TiO_2 at 2θ = 25.35°, 37.84°, 48.14°, 53.97°, and 55.18°. The hematite phase of α-Fe_2O_3 (JCPDS 73-2234) contains peaks at 2θ = 24.16°, 33.18°, 35.65°, 40.88°, 49.49°, 54.10°, 62.47°, and 64.04°, for which can be attributed to (012), (104), (101), (113),

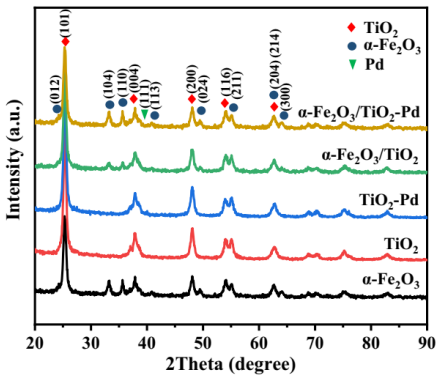

Fig. 2 XRD patterns of pure α-Fe_2O_3, TiO_2, TiO_2-Pd, α-Fe_2O_3/TiO_2 and α-Fe_2O_3/TiO_2-Pd

Table 1 The average crystallite size, crystallinity, and band gap energy of various samples

Sample	Average crystallite size (nm)	Crystallinity (%)	Band gap energy (E_g, eV)
TiO_2	19.01 ± 4.95	95.01	3.16
α-Fe_2O_3	21.78 ± 4.36	65.82	2.02
TiO_2-Pd	20.66 ± 2.02	95.54	3.14
α- Fe_2O_3/TiO_2	23.50 ± 6.65	92.55	2.18
α-Fe_2O_3/TiO_2-Pd	22.11 ± 3.56	94.54	2.00

(024), (116), (214), and (300), respectively. The XRD patterns of α-Fe_2O_3/TiO_2-Pd samples confirm that they contain hematite phase of α-Fe_2O_3 and anatase phase of TiO_2, which agrees with a previous study [38].The XRD pattern of Pd nanoparticles shows a peak at 2θ = 39.98° representing a lattice plane (111). The loading of Pd nanoparticles did not display any change in XRD peaks, possibly because of the small particle size and/or the low loading level on the TiO_2, as also reported in previous studies [50, 61]. However, the presence of Pd doping could be confirmed by XPS spectrum, which will be further discussed in the following section.

Table 1 shows the average crystallite size, the crystallinity, and band gap energy of various samples. The reported crystallite size is an average from replicate measurement. The average crystallite size of α-Fe_2O_3/TiO_2 photocatalyst was slightly increased from those of α-Fe_2O_3 and TiO_2 nanoparticles [49]. Loading Pd on α-Fe_2O_3/TiO_2 resulted in smaller crystallite size, which helps increasing surface area for photocatalytic activity [45]. The crystallinities of pure TiO_2 and α-Fe_2O_3 were 95.01% and 65.82%, respectively, while crystallinity was 92.55% for α-Fe_2O_3/TiO_2 sample. After loading Pd nanoparticles onto the heterojunction α-Fe_2O_3/TiO_2 surfaces, the average crystallinity was increased to 94.54%. The high crystallinity is expected to enhance the photocatalytic activity by improving the separation of photoinduced e^-–h^+ pairs [23, 62].

The band gap energy (E_g) was reduced when α-Fe_2O_3 and Pd were added onto the TiO_2 surface, as shown in Table 1. E_g = 2.18 and 2.00 eV were recorded for α-Fe_2O_3/TiO_2 and α-Fe_2O_3/TiO_2-Pd, respectively. The decreasing of E_g of TiO_2 (3.16 eV) to 2.00 eV in α-Fe_2O_3/TiO_2-Pd indicates the decrease in e^-–h^+ recombination rate under solar light.

The UV–Vis DSR data of TiO_2, TiO_2-Pd, and α-Fe_2O_3/TiO_2-Pd are shown in Fig. 3a. Pure TiO_2 and TiO_2-Pd showed absorption only in the UV range (< 400 nm) at energies exceeding their band gap energy (3.16 and 3.14 eV, respectively, Table 1). On the other hand, α-Fe_2O_3 showed strong light absorption over the visible range (λ ≥ 420 nm). The α-Fe_2O_3/TiO_2 heterostructures displayed significantly enhanced absorption in the visible region from 400 to 800 nm, and the high absorption window expanded when α-Fe_2O_3 was loaded onto the TiO_2 nanoparticles. In the heterojunction α-Fe_2O_3/TiO_2 composites, the visible light absorption is caused by $2(^6A_1) \rightarrow (^4T_1)$ ligand field transitions of Fe^{3+} [38].Compared to heterojunction α-Fe_2O_3/TiO_2, the heterojunction of α-Fe_2O_3/TiO_2-Pd ternary nanocomposite shows the larger visible light absorption region, which should improve photocatalytic activity as a stronger absorption intensity tends to improve the performance of photogenerated carriers. Tauc plots for TiO_2, TiO_2/Pd, α-Fe_2O_3, and α-Fe_2O_3/TiO_2 samples are shown in Fig. 3b–c. Tauc plots of α-Fe_2O_3/TiO_2-Pd in Fig. 3d confirms the reduction of the band gap energy in the ternary heterojunction α-Fe_2O_3/TiO_2-Pd nanocomposite.

The band gaps and corresponding valence band potential (E_{VB}) were determined from the XPS spectra of TiO_2 and α-Fe_2O_3 following a procedure reported by Bhoi et al. [63]. The E_{VB} is 2.78 eV and 1.39 eV for TiO_2 and α-Fe_2O_3, respectively. The conduction band potential (E_{CB}) value of TiO_2 is more positive than that of α-Fe_2O_3 (− 0.27 eV and − 0.63 eV relative to the Fermi level) [63, 64]. Therefore, the energy level potentials of TiO_2 and α-Fe_2O_3 in photocatalyst could be combined to form a heterojunction of α-Fe_2O_3/TiO_2 for photogenerated charge-separation and transfer [65].

The flat band potentials (V_{fb}) of TiO_2, α-Fe_2O_3, α-Fe_2O_3/TiO_2 and α-Fe_2O_3/TiO_2-Pd as determined by Mott-Schottky plots (Fig S2) were 0.73, − 0.31, − 0.33 and − 0.37 V (vs. Ag/AgCl), respectively. The slopes of all photocatalyzed samples (except TiO_2) are negative, which corresponding to the p-type of semiconductor [8]. The V_{fb} (vs. Ag/AgCl) obtained from the reference electrode was conversed to reversible hydrogen electrodes (RHE) and normal potential (NHE) unit

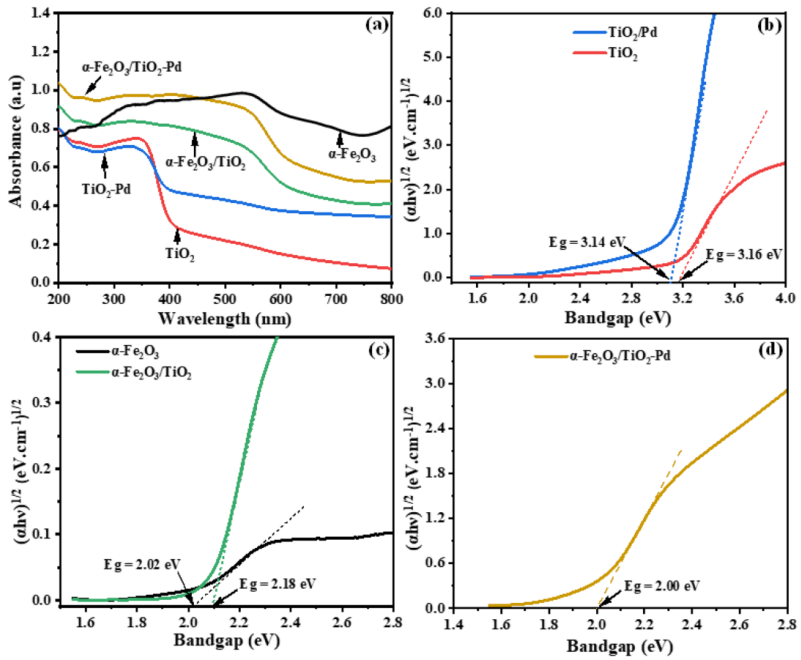

Fig. 3 **a** UV–Vis absorption spectra; and Tauc plots of **b** TiO_2 and TiO_2/Pd, **c** α-Fe_2O_3, α-Fe_2O_3/TiO_2, and **d** α-Fe_2O_3/TiO_2-Pd

Table 2 The flat band potential, conduction band, and valence band values as obtained from Mott-Schottky plots

Samples	Flat band potential (V_{fb}) (vs. Ag/AgCl)	Conduction band (E_{CB}) (vs. NHE)	Valence band (E_{VB}) (vs. NHE)
TiO_2	0.73	0.92	4.09
α-Fe_2O_3	−0.31	−0.11	1.91
α-Fe_2O_3/TiO_2	−0.33	−0.13	2.05
α-Fe_2O_3/TiO_2-Pd	−0.37	−0.17	1.83

following the procedure advised in a previous study [16]. Table 2 presents the potential of conduction band (E_{CB}) of TiO_2, α-Fe_2O_3, α-Fe_2O_3/TiO_2 and α-Fe_2O_3/TiO_2-Pd, which corresponds to 0.92, − 0.11, − 0.13, and − 0.17 (vs. NHE), respectively. The potential of valence band (E_{VB}) of TiO_2, α-Fe_2O_3, α-Fe_2O_3/TiO_2 and Fe_2O_3/TiO_2-Pd was determined to be 4.09, 1.91, 2.05, and 1.83 (vs. NHE), respectively. The smaller E_{CB} and E_{VB} values obtained in α-Fe_2O_3/TiO_2-Pd sample indicates the superior capability to enhance charge

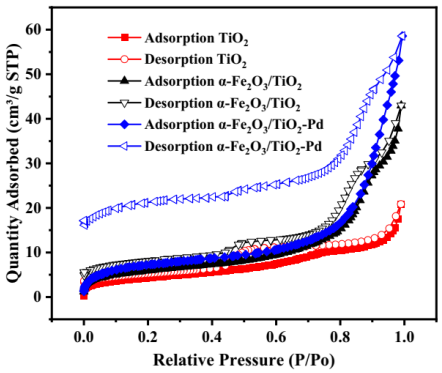

Fig. 4 Nitrogen adsorption–desorption isotherms of TiO_2, α-Fe_2O_3/TiO_2 and α-Fe_2O_3/TiO_2-Pd

carrier separation and the decrease in driving force for a specific photocatalytic reaction [8, 16].

The nitrogen adsorption-deposition isotherms are shown in Fig. 4. The textural properties including BET specific surface area, average pore diameter, and average pore volume for the photocatalyst samples are summarized in Table 3. The isotherm obtained from the pure TiO_2 fit well with the type V isotherm curve, while the isotherms of the α-Fe_2O_3/TiO_2 and α-Fe_2O_3/TiO_2-Pd exhibited a type IV isotherm. These results are similar to the results obtain by Khasawneh et al. [51]. The hysteresis loops are H3 type according to IUPAC classification at the high relative pressure for α-Fe_2O_3/TiO_2-Pd [66]. This result indicates that all types of catalyst contain mesoporous structure with the narrow pore size between 8 and 14 nm. [66, 67]. The BET specific surface area (SSA) was 15.68, 21.05 and 25.51 m^2/g for TiO_2 and α-Fe_2O_3/TiO_2, and α-Fe_2O_3/TiO_2-Pd, respectively (Table 3). The incorporation of Pd ternary with TiO_2 has significantly increased SSA, crystallinity, and surface activity on α-Fe_2O_3. Meanwhile, 1%Pd incorporation resulted in 13% and 27% increase in the average pore size and the average pore volume, respectively. Therefore, the highest BET specific area and pore diameter observed in the ternary of α-Fe_2O_3/TiO_2-Pd indicates an improve in photocatalyst properties.

Table 3 BET surface area, average pore diameter, and average pore volume of samples

Sample	BET surface area (BET, m^2/g)	Average pore diameter (nm)	Average pore volume (cm^3/g)
TiO_2	15.68	8.22	0.032
TiO_2/Pd	13.25	9.41	0.031
α-Fe_2O_3/TiO_2	21.05	12.62	0.066
α-Fe_2O_3/TiO_2-Pd	25.51	14.20	0.090

The recombination and separation efficiency of charge carriers was investigated from PL spectra as shown in Fig. 5a. The strong PL intensity was observed for pure TiO_2, indicating that the electrons and holes recombined rapidly [44, 68]. The emission intensity of photocatalyst

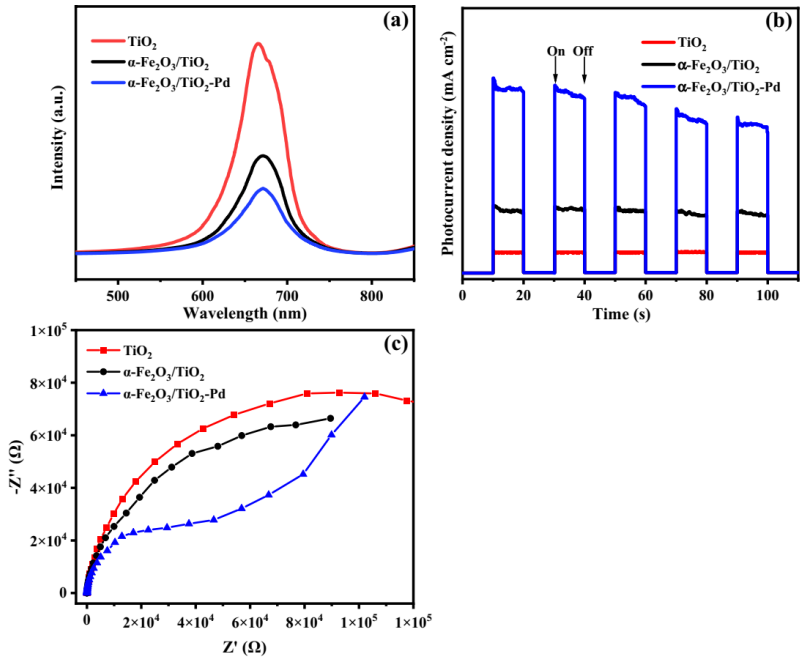

Fig. 5 **a** PL spectra of TiO_2, α-Fe_2O_3/TiO_2 and α-Fe_2O_3/TiO_2-Pd, **b** Photocurrent response curve, and **c** EIS Nyquist plots of TiO_2, α-Fe_2O_3/TiO_2 and α-Fe_2O_3/TiO_2-Pd under visible light irradiation

heterojunction α-Fe_2O_3/TiO_2 nanocomposite was lower than that of pure TiO_2, indicating that the recombination rate of electron–hole pairs was reduced for photocatalyst nanocomposite sample. A lower PL intensity indicates lower recombination rate and higher photocatalyst activity [64, 69]. After loading Pd nanoparticles on α-Fe_2O_3/TiO_2 nanocomposite, the emission intensity of α-Fe_2O_3/TiO_2-Pd was lower than that of α-Fe_2O_3/TiO_2 photocatalyst, which indicates that the Pd effectively inhibited the e^-–h^+ recombination [70]. Therefore, the loading of Pd nanoparticles can improve charge separation efficiency in photocatalytic applications. To confirm the separation and migration, photogenerated charge carriers in pure TiO_2, α-Fe_2O_3/TiO_2 and α-Fe_2O_3/TiO_2-Pd photocatalyst materials were measured by photocurrent response as shown Fig. 5b. The photocurrent of the pure TiO_2 was found to be the lowest, indicating the rapid recombination of photogenerated charge carrier. The photocurrent response of the ternary heterojunction α-Fe_2O_3/TiO_2-Pd nanocomposite was much greater than that of pure TiO_2 and α-Fe_2O_3/TiO_2 (α-Fe_2O_3/TiO_2-Pd > α-Fe_2O_3/TiO_2 > TiO_2), which is an evidence of a more efficient separation of photogenerated e^-–h^+ pair [64, 67]. The EIS Nyquist of TiO_2, α-Fe_2O_3/TiO_2 and α-Fe_2O_3/TiO_2-Pd were 17.2 kΩ, 15.7 kΩ and 10.3 kΩ, respectively (Fig. 5c). The EIS Nyquist plot of TiO_2 exhibited a higher semicircle curve, suggesting the highest resistance of charge transfer compared to those of α-Fe_2O_3/TiO_2 and α-Fe_2O_3/TiO_2-Pd. The α-Fe_2O_3/TiO_2-Pd curve had small radius circle, for which indicates a lower resistance for charge transfer and a lower e^-–h^+ recombination rate [45, 57]. It can be concluded that Pd nanoparticle deposited on α-Fe_2O_3/TiO_2 could provide a more efficient interfacial charge transfer according to the mesostructured, high SSA, and at the same time also reduce the e^-–h^+recombination.

The morphology of TiO_2, Fe_2O_3 and α-Fe_2O_3/TiO_2-Pd nanocomposites was characterized by FE-SEM and TEM. In Fig. 6a, the morphology of TiO_2 shows an average diameter in the range of 50–100 nm and an average length of 5–7 µm, which agrees well with number published in prior reports [38, 71]. The morphology of α-Fe_2O_3 is shown in Fig. 6b, for which illustrate the average diameter of α-Fe_2O_3 of 500 nm. According to a previous study [50], for α-Fe_2O_3/TiO_2 nanocomposite, α-Fe_2O_3 was deposited densely and combined tightly onto the TiO_2 surfaces to form heterojunctions between these two materials. In this study, we found that the Pd composite did not cause any significant change in the structure of the heterojunctions of α-Fe_2O_3/TiO_2 nanocomposite as observed in Fig. 6c and d. A typical TEM image of heterojunction α-Fe_2O_3/TiO_2-Pd ternary nanocomposites (Fig. 6e) and the existence of the lattice spacings of 0.35 and 0.25 nm (Fig. 6f–h) can be attributed to (101) and (110) crystal planes of anatase TiO_2 and α-Fe_2O_3, respectively [49]. Meanwhile, Pd demonstrated lattice spacing of

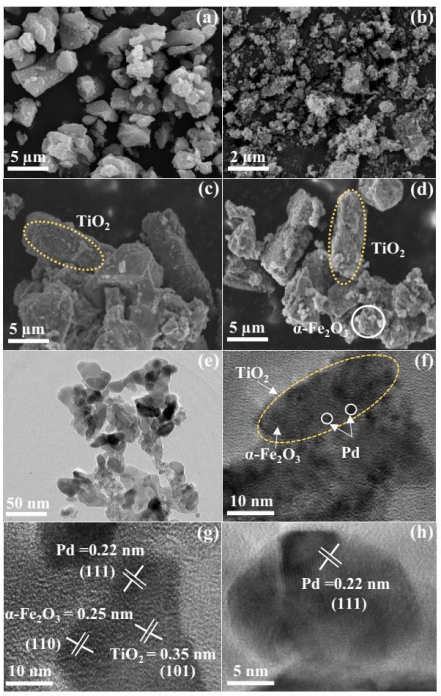

Fig. 6 FE-SEM images of **a** TiO_2, **b** α-Fe_2O_3, **c**, **d** α-Fe_2O_3/TiO_2-Pd, and **e–h** TEM images of α-Fe_2O_3/TiO_2-Pd

0.22 nm that corresponds to the (111) plane of the metal itself [61].

The EDS results of the α-Fe_2O_3/TiO_2-Pd photocatalytic nanocomposites are presented in Fig. 7a, b, which confirm the presence of Fe and Pd elements on the surfaces of TiO_2. The elemental composition of Ti, O, C, Fe, and Pd were found to be 42.4, 36.6, 10.9, 9.5, and 0.7 wt% respectively. The elemental EDS mapping images of Ti, Fe, and Pd in Fig. 7c–e clearly demonstrate that TiO_2, α-Fe_2O_3, and Pd were uniformly distributed on the photocatalyst surfaces.

The chemical states of elements in the α-Fe_2O_3/TiO_2-Pd ternary heterojunction photocatalysts were measured by using high-resolution XPS. In Fig. 8a, the survey scan illustrates the presence of Ti, O, Fe, and Pd elements. The high-resolution Ti scan in Fig. 8b indicates two binding peaks at 464.2 and 458.5 eV, which correspond to Ti $2p_{1/2}$ and Ti $2p_{3/2}$, respectively. The split between Ti $2p_{1/2}$ and Ti $2p_{3/2}$ (5.7 eV) indicated the normal state of Ti^{4+} [37, 72]. The Ti $2p_{1/2}$ peak at 458.5 eV was caused by the

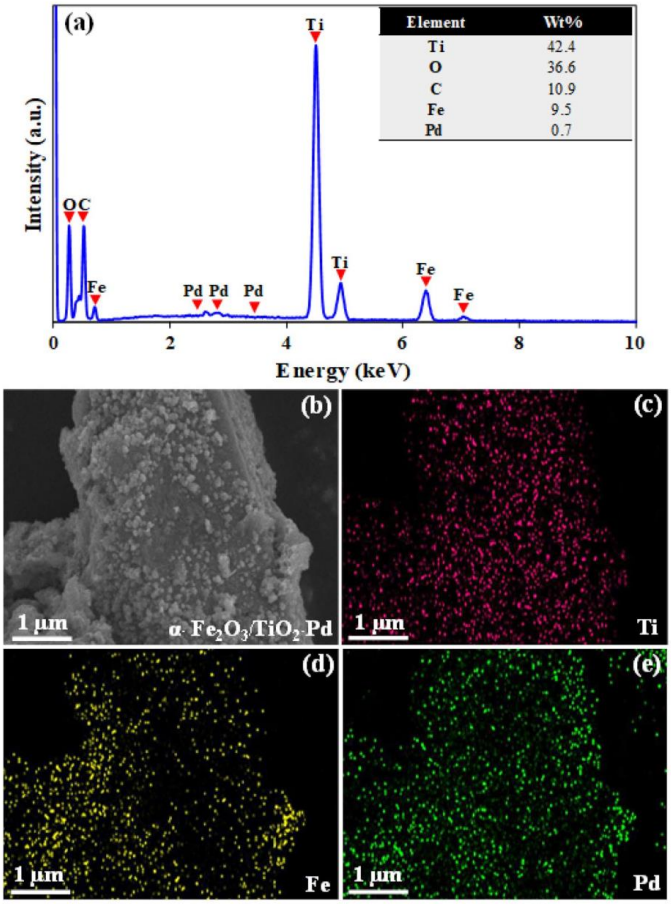

Fig. 7 EDS mapping spectrum of **a** α-Fe_2O_3/TiO_2-Pd photocatalyst, and EDS mapping images of **b** α-Fe_2O_3/TiO_2-Pd, **c** Ti, **d** Fe, and **e** Pd

formation of Fe–O–Ti bonds in the α-Fe_2O_3/TiO_2 [73]. In Fig. 8c, the binding energies of Fe at 711.3 and 724.8 eV correspond to Fe $2p_{3/2}$ and Fe $2p_{1/2}$ of Fe_2O_3, respectively. A shakeup satellite peak at 719.1 eV occurred due to the Fe^{3+} in α-Fe_2O_3 [19]. In Fig. 8d, the Pd 3d spectrum shows two peaks with the binding energies of 338.1 and 343.5 eV, which are assigned to Pd $3d_{5/2}$ and Pd $3d_{3/2}$ of metallic Pd [74], respectively. Hence, the Pd element was successfully deposited onto the heterojunction of α-Fe_2O_3/TiO_2 as a ternary. The O 1s spectrum displayed component lattice cantered at 529.1 eV, and two binding peaks at 531.3 and 532.2 eV, which attributed to oxygen species (OH^-) (Fig S1) [50] bonded to Ti–O (titanium) and Fe–O (iron) [38, 50]. All of the above results indicate that the ternary heterojunctions in α-Fe_2O_3/TiO_2-Pd nanocomposite were synthesized successfully.

3.2 H_2 Production

The photocatalytic H_2 production rates from water and a sacrificial agent over different TiO_2-based photocatalysts are presented in Fig. 9a. The H_2 production rate was at 40.12 µmol.h^{-1} g^{-1} for anatase TiO_2. This low production rate indicates poor photocatalytic activity of pure TiO_2. The

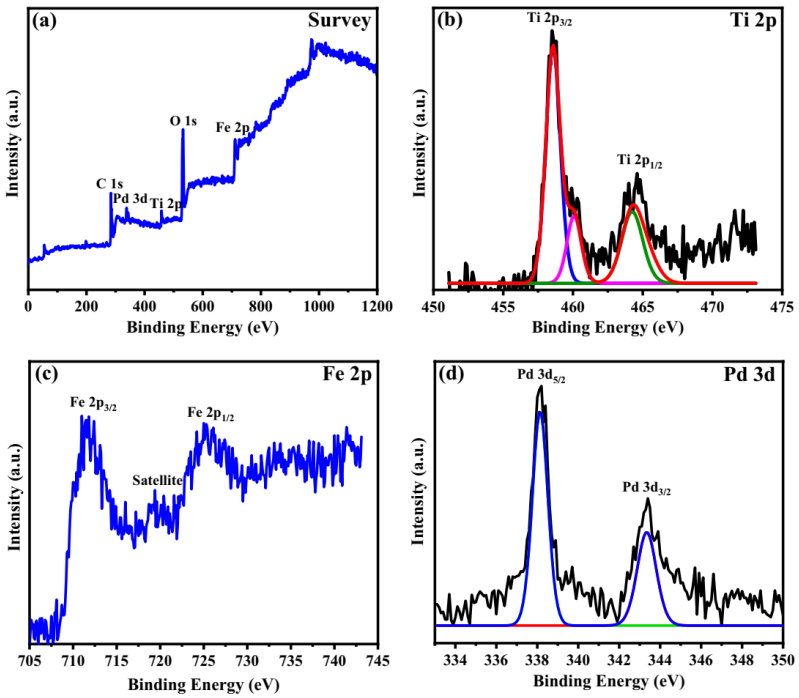

Fig. 8 XPS survey spectrum of **a** α -Fe_2O_3/TiO_2-Pd and high-resolution spectra of **b** Ti 2p, **c** Fe 2p, and **d** Pd 3d

H_2 production rate of 1400.91 μmol.h^{-1} g^{-1} was achieved for TiO_2/Pd with UV light. After loading α-Fe_2O_3 onto the TiO_2 surface, the production rate of 740.60 μmol.h^{-1} g^{-1} was obtained. In comparison, ternary heterojunction α-Fe_2O_3/TiO_2-Pd samples showed a significantly higher H_2 production rate at 3490.54 μmol.h^{-1} g^{-1}, corresponds to an increase of 78.65% compared to α-Fe_2O_3/TiO_2. Hence, the highest H_2 production rate was observed with the ternary heterojunction α-Fe_2O_3/TiO_2-Pd nanocomposite.

The effects of irradiation time on H_2 production using different samples are presented in Fig. 9b. The pure TiO_2 anatase corresponded to a low H_2 production rate at due to its rapid recombination of photogenerated e^-–h^+ pairs [75]. The α-Fe_2O_3/TiO_2 also exhibited a lower photocatalyst activity in the beginning because of the recombination of photogenerated charge carriers, but the H_2 production gradually increased to 11,971 μmol g^{-1} after 6 h of irradiation. For α-Fe_2O_3/TiO_2-Pd, the H_2 production increased rapidly over irradiation time and reached 27,072 μmol g^{-1} after 6 h. These results of Pd acting as a co-catalyst enhancing photocatalysis activity were based on electron transfer charge carrier and separation functions.

After 4-h cycle of H_2 production, the photocatalyst was cleaned and dried to be reused again. The stability of ternary α-Fe_2O_3/TiO_2-Pd photocatalyst in H_2 production was evaluated and the results are shown in Fig. 9c. After 5 cycles over the 20-h period, α-Fe_2O_3/TiO_2-Pd photocatalyst still exhibited a good photocatalytic stability in H_2 production. Thus, the presence of ternary Pd improved the stability of H_2 production. Liu et al. [50] also reported that the Fe_2O_3-TiO_2-Pt nanocomposite had excellent stability in H_2 production. However, the H_2 production rate for α-Fe_2O_3/TiO_2-Pd photocatalyst slightly decreased with reaction cycles. 10% reduction after five cycles was observed. This finding is in accordance with a previous study [50] reporting that the photocatalytic rate was slightly reduced during the long-term reaction, possibly by the formation of Pd oxide [70].

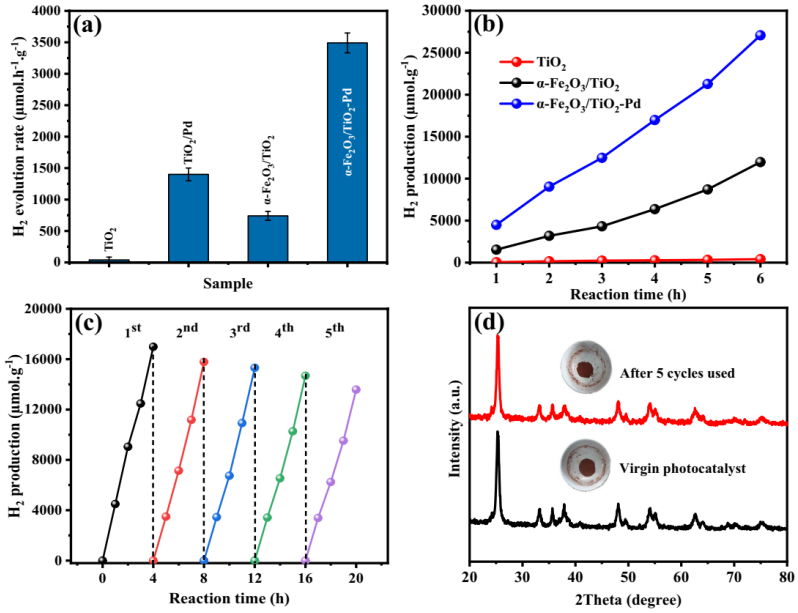

Fig. 9 **a** Hydrogen evolution from different photocatalysts, **b** hydrogen production over a long irradiation time, **c** stability of α-Fe_2O_3/TiO_2-Pd after recycling, and **d** XRD assessment after recycling

The XRD patterns of the virgin α-Fe_2O_3/TiO_2-Pd photocatalyst and the one after 5 consecutive cycles of photocatalytic reactions are shown in Fig. 9d. There is no drastic change observed between the characteristic peaks of the virgin and used samples, which suggesting that these photocatalyst nanocomposites have good long-term stability and reusability [44]. We concluded that the presence of Pd ternary deposition over the heterojunction of α-Fe_2O_3/TiO_2 enhanced the photocatalytic activity as well as the stability of photocatalyst.

Table 4 compares H_2 production rate from the results of several studies under similar experimental conditions but with different noble metals used as co-catalysts. The H_2 production rate from Pt ternary loaded onto TiO_2–Fe_2O_3 nanocomposite under visible light irradiation and MeOH as sacrificial agent was at 90 μmol h^{-1} [50], while Au [76] or Pd [77] loaded onto TiO_2/graphene nanocomposite corresponded to H_2 production rate of 296 and 280.8 μmol h^{-1}, respectively. The hydrogen production rate measured in this study is higher than those in previous studies [76, 77] as the loaded ternary Pd on α-Fe_2O_3/TiO_2 heterojunction induced a higher photocatalytic activity. Moreover, the Pd loading could reduce the recombination of e^-–h^+, producing a higher charge transfer rate coefficient [37]. Therefore, it can be concluded that using Pd as a co-catalyst effectively enhances H_2 production.

In general, when heterojunction photocatalysts are developed from more than two semiconductors, they do not only allow a broad range of light absorption but also enhance charge separation by separating the electrons and holes to different semiconductors. The developed heterojunction can be categorized into type-II heterojunction or step-scheme (S-scheme) heterojunction. In this study, the possible mechanism is that α-Fe_2O_3 and TiO_2 form S-scheme heterojunction. The S-scheme heterojunction differs from a type-II heterojunction, as the charge-transfer mechanism of the S-scheme heterojunction comprise a reduction photocatalyst and an oxidation photocatalyst with staggered band structure [78].

As the work function of heterojunction photocatalyst was investigated, the interfacial charge transfers between α-Fe_2O_3 and TiO_2 of before contact, after contact, and light irradiation are shown in Fig. 10. Before contact, the work function of α-Fe_2O_3 and TiO_2 was previously reported to be

Table 4 H_2 production rate with different noble metals as co-catalysts on heterojunction photocatalysts

Heterojunction	Ternary	Sacrificial agent	Light Source	H_2 production (μmol h^{-1})	Refs
α-Fe_2O_3/TiO_2	Pd	Methanol	250 W, LED, λ ≥ 420 nm	349.5	This work
CdS/g-C_3N_4	Pd	Sodium sulfite	300 W, Xe λ ≥ 400 nm	293.0	[45]
TiO_2–Fe_2O_3	Pt	Methanol	300 W, Xe, λ ≥ 400 nm	90.0	[50]
TiO_2/GO	Au	Methanol	12 W, LED, λ ≥ 420 nm	296.0	[76]
TiO_2/GO	Pd	Methanol	288 W, Hg λ ≥ 400 nm	280.8	[77]
TiO_2/g-C_3N_4	Pt	Triethanolamine	300 W, Xe λ ≥ 420 nm	40.0	[81]
TiO_2–ZnO	Pt	Methanol	300 W, Hg λ ≥ 420 nm	215.0	[83]
TiO_2/V_2O_5	Pt	Methanol	125 W, Hg, λ ≥ 400 nm	296.6	[84]

GO graphene oxide, *Xe* xenon lamp, *Hg* mercury lamp, V_2O_5 vanadium oxide, *g-*C_3N_4 graphitic carbon nitride, *ZnO* zinc oxide and Na_2S sodium sulphide

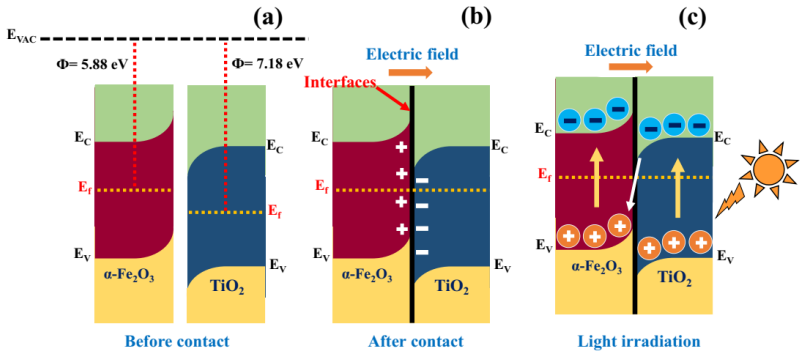

Fig. 10 S-scheme α-Fe_2O_3 and TiO_2 pathway of charge carrier: **a** the work function before contact, **b** after contact and **c** light irradiation of S-scheme heterojunction

5.88 eV [79] and 7.18 eV [80], respectively (Fig. 10a). After contact (Fig. 10b), the difference of work function indicated the electron transfer from α-Fe_2O_3 to TiO_2 as Fermi energy of TiO_2 was lower than that of α-Fe_2O_3 [79, 80]. TiO_2 has a greater work function, which indicates that charge transfer occurred at the interface from α-Fe_2O_3 to TiO_2, relative to the equilibrium of the Fermi energies [40]. The charge transfer led to an increase of electrons density at TiO_2 and a decrease of electrons density at α-Fe_2O_3 at the interface. This result indicates a built-in electric field between α-Fe_2O_3 and TiO_2 at the interface. Under light irradiation (Fig. 10c), electrons are excited from CB of TiO_2, then the electrons were transferred to VB of α-Fe_2O_3 and recombined with the hole in VB of Fe_2O_3. Simultaneously, the recombination of electrons and hole in CB of α-Fe_2O_3 and VB of TiO_2 can be prevented, for which enhanced the photogenerated charge carrier [58].

The mechanism of heterojunction electron transfer in ternary of α-Fe_2O_3/TiO_2-Pd under visible light irradiation for H_2 generation is shown in Fig. 11. When visible light is irradiated on the heterojunction of α-Fe_2O_3/TiO_2-Pd nanocomposite, the photogenerated electrons in the CB of α-Fe_2O_3 are transferred

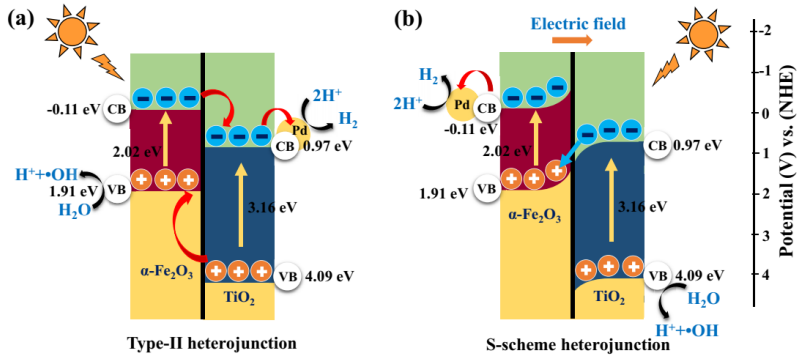

Fig. 11 Mechanism of photocatalysis over α-Fe_2O_3/TiO_2-Pd under visible light: **a** type-II heterojunction and **b** S-scheme heterojunction

to the CB of TiO_2, while the holes show a reverse transfer route [45, 78]. Furthermore, these electrons migrate to Pd on the crystallite surface in the CB of TiO_2 and accumulate there, forming a Schottky barrier between the Pd nanoparticle as ternary on the surface of α-Fe_2O_3/TiO_2 [44, 81]. The photogenerated holes in the VB reacted with water to create pairs of the proton (H^+) and hydroxyl radical (·OH) [33]. The generated H^+ will recombine with free electrons from Pd to form H atom and subsequently the H_2 molecule. By allowing the ·OH to react with the sacrificial agent methanol, the timescale of separation for the photogenerated electrons and holes is prolonged. TiO_2 has a larger work function (7.18 eV) with an oxidation-type, while α-Fe_2O_3 (5.88 eV) has a smaller work function with reduction-type of photocatalysts. The mechanism of ternary of α-Fe_2O_3/TiO_2-Pd as explained by the S-scheme heterojunction is that the electron in the VB of α-Fe_2O_3 and TiO_2 are transferred to CB of each photocatalyst. Meanwhile, the electrons in the CB of TiO_2 are easily transferred to the VB of α-Fe_2O_3, because the driving force of the electric field at in the interface [80, 82]. Thus, the photogenerated electrons in CB of α-Fe_2O_3 can migrate to Pd, which increase the redox ability for H_2 production, the photogenerated h^+ in the VB of TiO_2 involves H_2O oxidation and increase the separation of photogenerated e^-–h^+ pairs based on the results discussed earlier. Therefore, the results indicate that the ternary heterojunction of α-Fe_2O_3/TiO_2-Pd was a typical S-Scheme system as shown in Fig. 11b.

4 Conclusions

In summary, the new S-scheme α-Fe_2O_3/TiO_2 heterojunctions with ternary Pd nanoparticles were successfully synthesized in this work to use in H_2 production through water splitting.

- The heterojunction α-Fe_2O_3/TiO_2-Pd ternary nanocomposites achieved absorption in the range of visible light, high-efficiency in the separation of e^-–h^+ pairs, and stable performance in the multi-cycle reaction for H_2 production. The Pd ternary reduced the e^-–h^+ recombination rates, which leads to higher charge transfer and H_2 production rates.
- The ternary Pd nanoparticle loading on heterojunction α-Fe_2O_3/TiO_2 exhibited great performance, with H_2 production rate of 3490.45 μmol h^{-1} and excellent stability in multi-cycle H_2 production. Therefore, the experimental results and theoretical analyses confirm the high potential for the applicability of the new photocatalysts for hydrogen production through photocatalytic water splitting.

Supplementary Information The online version contains supplementary material available at https://doi.org/10.1007/s10562-021-03873-5.

Acknowledgements This research study was financially supported by the Inter-disciplinary Graduate School of Energy Systems (IGS-Energy), Graduate School of Prince of Songkla University and the Center of Excellence in Membrane Science and Technology, Prince of Songkla University. This work was partially conducted under the research on development of novel technologies for safe agriculture by Faculty of Engineering, Khon Kaen University which has received funding support from Fundamental Fund 2022 (the National Science, Research and Innovation Fund (NSRF), Thailand). The authors were grateful thanks Assoc. Prof. Seppo Karrila and Publication Clinic, Research and Develop Office for English proved.

References

1. Bezdek RH (2019) The hydrogen economy and jobs of the future. Renew Energy Environ Sustain 4:1. https://doi.org/10.1051/rees/2018005
2. Luo M, Yi Y, Wang S, Wang Z, Du M, Pan J, Wang Q (2018) Review of hydrogen production using chemical-looping technology. Renew Sustain Energy Rev 81:3186–3214. https://doi.org/10.1016/j.rser.2017.07.007
3. Montini T, Monai M, Beltram A, Romero OI, Fornasiero P (2016) H_2 production by photocatalytic reforming of oxygenated compounds using TiO_2-based materials. Mater Sci Semicond Process 42:122–130. https://doi.org/10.1016/j.mssp.2015.06.069
4. Melián EP, Díaz OG, Méndez AO, López CR, Suárez MN, Rodríguez JMD, Navío JA, Hevia DF, Peña JP (2013) Efficient and affordable hydrogen production by water photo-splitting using TiO_2 based photocatalysts. Int J Hydrogen Energy 38:2144–2155. https://doi.org/10.1016/j.ijhydene.2012.12.005
5. Safari F, Dincer I (2019) Development and analysis of a novel biomass based integrated system for multigeneration with hydrogen production. Int J Hydrogen Energy 44:3511–3526. https://doi.org/10.1016/j.ijhydene.2018.12.101
6. Huang CW, Nguyen BS, Wu JCS, Nguyen VH (2019) A current perspective for photocatalysis towards the hydrogen production from biomass derived organic substances and water. Int J Hydrogen Energy. https://doi.org/10.1016/j.ijhydene.2019.08.121
7. Wang Z, Roberts RR, Naterer GF, Gabriel KS (2012) Comparison of thermochemical, electrolytic, photoelectrolytic and photochemical solar to hydrogen production technologies. Int J Hydrogen Energy 37:16287–16301. https://doi.org/10.1016/j.ijhydene.2012.03.057
8. Atacan K, Güy N, Boutra B, Özacar M (2020) Enhancement of photoelectrochemical hydrogen production by using a novel ternary Ag_2CrO_4/GO/$MnFe_2O_4$ photocatalyst. Int J Hydrogen Energy 45:17453–17467. https://doi.org/10.1016/j.ijhydene.2020.04.268
9. Habibi YA, Asadzadeh KS, Feizpoor S, Rouhi A (2020) Review on heterogeneous photocatalytic disinfection of waterborne, airborne, and foodborne viruses: can we win against pathogenic viruses? J Colloid Interface Sci 580:503–514. https://doi.org/10.1016/j.jcis.2020.07.047
10. Asadzadeh KS, Habibi YA (2020) g-C_3N_4/carbon dot-based nanocomposites serve as efficacious photocatalysts for environmental purification and energy generation: a review. J Clean Prod 276:124319. https://doi.org/10.1016/j.jclepro.2020.124319
11. Burgess G, Fernández VJG (2007) Materials, operational energy inputs, and net energy ratio for photobiological hydrogen production. Int J Hydrogen Energy 32:1225–1234. https://doi.org/10.1016/j.ijhydene.2006.10.055
12. Qureshy AMMI, Ahmed M, Dincer I (2019) Performance assessment study of photoelectrochemical watersplitting reactor designs for hydrogen production. Int J Hydrogen Energy 44:9237–9247. https://doi.org/10.1016/j.ijhydene.2019.01.280
13. Wang H, Zhang L, Chen Z, Hu J, Li S, Wang Z, Liu J, Wang X (2014) Semiconductor heterojunction photocatalysts: design, construction, and photocatalytic performances. Chem Soc Rev 43:5234–5244. https://doi.org/10.1039/c4cs00126e
14. Iglesias O, Rivero MJ, Urtiaga AM, Ortiz I (2016) Membrane based photocatalytic systems for process intensification. Chem Eng J 305:136–148. https://doi.org/10.1016/j.cej.2016.01.047
15. Molinari R, Lavorato C, Argurio P (2015) Photocatalytic reduction of acetophenone in membrane reactors under UV and visible light using TiO_2 and Pd/TiO_2 catalysts. Chem Eng J 274:307–316. https://doi.org/10.1016/j.cej.2015.03.120
16. Güy N, Atacan K, Yıldırım İ, Özacar M (2021) Insight into the efficient photocatalytic removal mechanism of organic pollutants by plasmonic Z-scheme MoS_2/Ag/Ag_3VO_4 heterojunction under visible light. J Mol Liq. https://doi.org/10.1016/j.molliq.2021.115311
17. Gan W, Zhang J, Niu H, Bao L, Hao H, Yan Y, Wu K, Fu X (2019) Fabrication of Ag/AgBr/TiO_2 composites with enhanced solar-light photocatalytic properties. Colloids Surf A Physicochem Eng Asp 583:123968. https://doi.org/10.1016/j.colsurfa.2019.123968
18. Fajrina N, Tahir M (2019) A critical review in strategies to improve photocatalytic water splitting towards hydrogen production. Int J Hydrogen Energy 44:540–577. https://doi.org/10.1016/j.ijhydene.2018.10.200
19. Li X, Lin H, Chen X, Niu H, Jiuyu L, Zhang T, Qu F (2016) Dendritic α-Fe_2O_3/TiO_2 nanocomposites with improved visible light photocatalytic activity. Phys Chem Chem Phys 18:9176–9185. https://doi.org/10.1039/c5cp06681f
20. Rosman NN, Mohamad YR, Jeffery ML, Arifin K, Salehmin MNI, Mohamed MA, Kassim MB (2018) Photocatalytic properties of two-dimensional graphene and layered transition-metal dichalcogenides based photocatalyst for photoelectrochemical hydrogen generation: an overview. Int J Hydrogen Energy 43:18925–18945. https://doi.org/10.1016/j.ijhydene.2018.08.126
21. Ahmad H, Kamarudin SK, Minggu LJ, Kassim M (2015) Hydrogen from photocatalytic water splitting process: a review. Renew Sustain Energy Rev 43:599–610. https://doi.org/10.1016/j.rser.2014.10.101
22. Jafari T, Moharreri E, Amin AS, Miao R, Song W, Suib SL (2016) Photocatalytic water splitting - The untamed dream: a review of recent advances. Molecules 21:900. https://doi.org/10.3390/molecules21070900
23. Chiarello GL, Dozzi MV, Selli E (2017) TiO_2 based materials for photocatalytic hydrogen production. J Energy Chem 26:250–258. https://doi.org/10.1016/j.jechem.2017.02.005
24. Kumaravel V, Mathew S, Bartlett J, Pillai SC (2019) Photocatalytic hydrogen production using metal doped TiO_2: a review of recent advances. Appl Catal B Environ 244:1021–1064. https://doi.org/10.1016/j.apcatb.2018.11.080
25. Ismail AA, Bahnemann DW (2014) Photochemical splitting of water for hydrogen production by photocatalysis: a review. Sol Energy Mater Sol Cells 128:85–101. https://doi.org/10.1016/j.solmat.2014.04.037
26. Schneider J, Matsuoka M, Takeuchi M, Zhang J, Horiuchi Y, Anpo M, Bahnemann DW (2014) Understanding TiO_2 photocatalysis: mechanisms and materials. Chem Rev 114:9919–9986. https://doi.org/10.1021/cr5001892
27. Reza GM, Dinh CT, Béland F, Do TO (2015) Nanocomposite heterojunctions as sunlight-driven photocatalysts for hydrogen production from water splitting. Nanoscale 7:8187–8208. https://doi.org/10.1039/c4nr07224c
28. Wei L, Yu C, Zhang Q, Liu H, Wang Y (2018) TiO_2 based heterojunction photocatalysts for photocatalytic reduction of CO_2 into solar fuels. J Mater Chem A 6:22411–22436. https://doi.org/10.1039/c8ta08879a

29. Fawzi SKO, Palaniandy P (2020) Removal of organic pollutants from water by Fe_2O_3/TiO_2 based photocatalytic degradation: a review. Environ Technol Innov 21:101230. https://doi.org/10.1016/j.eti.2020.101230
30. Mishra M, Chun DM (2015) α-Fe_2O_3 as a photocatalytic material: a review. Appl Catal A Gen 498:126–141. https://doi.org/10.1016/j.apcata.2015.03.023
31. Li N, Tang S, Rao Y, Qi J, Wang P, Jiang Y, Huang H, Gu J, Yuan D (2018) Improved dye removal and simultaneous electricity production in a photocatalytic fuel cell coupling with persulfate activation. Electrochim Acta 270:330–338. https://doi.org/10.1016/j.electacta.2018.03.083
32. Wu L, Yan H, Xiao J, Li X, Wang X, Zhao T (2017) Characterization and photocatalytic properties of nano-Fe_2O_3–TiO_2 composites prepared through the gaseous detonation method. Ceram Int 43:14334–14339. https://doi.org/10.1016/j.ceramint.2017.07.189
33. Madhumitha A, Preethi V, Kanmani S (2018) Photocatalytic hydrogen production using TiO_2 coated iron-oxide core shell particles. Int J Hydrogen Energy 43:3946–3956. https://doi.org/10.1016/j.ijhydene.2017.12.127
34. Preethi V, Kanmani S (2014) Photocatalytic hydrogen production using Fe_2O_3 based core shell nano particles with ZnS and CdS. Int J Hydrogen Energy 39:1613–1622. https://doi.org/10.1016/j.ijhydene.2013.11.029
35. Li X, Wang Z, Zhang Z, Chen L, Cheng J, Ni W, Wang B, Xie E (2015) Light illuminated α-Fe_2O_3/Pt nanoparticles as water activation agent for. Sci Rep 5:1–7. https://doi.org/10.1038/srep09130
36. Yu L, Zhang Y, He J, Zhu H, Zhou X, Li M, Yang Q, Xu F (2018) Enhanced photoelectrochemical properties of α-Fe_2O_3 nanoarrays for water splitting. J Alloys Compd 753:601–606. https://doi.org/10.1016/j.jallcom.2018.04.258
37. Zhu S, Yao F, Yin C, Li Y, Peng W, Ma J, Zhang D (2014) Fe_2O_3/TiO_2 photocatalyst of hierarchical structure for H2 production from water under visible light irradiation. Microporous Mesoporous Mater 190:10–16. https://doi.org/10.1016/j.micromeso.2014.01.018
38. Huang R, Liang R, Fan H, Ying S, Wu L, Wang X, Yan G (2017) Enhanced photocatalytic fuel denitrification over TiO_2/α-Fe_2O_3 nanocomposites under visible light irradiation. Sci Rep 7:1–10. https://doi.org/10.1038/s41598-017-08439-3
39. Xie Q, He W, Liu S, Li C, Zhang J, Wong PK (2020) Bifunctional S-scheme g-C_3N_4/Bi/$BiVO_4$ hybrid photocatalysts toward artificial carbon cycling. Chin J Catal 41:140–153. https://doi.org/10.1016/S1872-2067(19)63481-9
40. Fu J, Xu Q, Low J, Jiang C, Yu J (2019) Ultrathin 2D/2D WO_3/g-C_3N_4 step-scheme H_2 production photocatalyst. Appl Catal B Environ 243:556–565. https://doi.org/10.1016/j.apcatb.2018.11.011
41. Zhu Y, Yang J, Bian C et al (2021) NiO decorated Ti/TiO_2 nanotube arrays (TiO_2NT)/TiO_2/g-C_3N_4 step-scheme heterostructure thin film photocatalyst with enhanced photocatalytic activity for water splitting. Catal Lett 151:3067–3078. https://doi.org/10.1007/s10562-021-03545-4
42. Hu T, Dai K, Zhang J, Chen S (2020) Noble metal free Ni_2P modified step-scheme $SnNb_2O_6$/CdS-diethylenetriamine for photocatalytic hydrogen production under broadband light irradiation. Appl Catal B Environ 269:118844. https://doi.org/10.1016/j.apcatb.2020.118844
43. Yan T, Liu H, Jin Z (2021) G-C_3N_4/α-Fe_2O_3 supported zero-dimensional CO_3S_4 nanoparticles form S-scheme heterojunction photocatalyst for efficient hydrogen production. Energy Fuels 35:856–867. https://doi.org/10.1021/acs.energyfuels.0c03351
44. Zhao Z, Cheng DG, Chen F, Zhan X (2020) Hierarchical porous TS-1/Pd/CdS catalysts for enhanced photocatalytic hydrogen evolution. Int J Hydrogen Energy 45:33532–33542. https://doi.org/10.1016/j.ijhydene.2020.09.099
45. Güy N (2020) Directional transfer of photocarriers on CdS/g-C_3N_4 heterojunction modified with Pd as a cocatalyst for synergistically enhanced photocatalytic hydrogen production. Appl Surf Sci 522:146442. https://doi.org/10.1016/j.apsusc.2020.146442
46. Ramírez OD, Guerrero AD, Acevedo PP, Lartundo RL, Zanella R (2020) Effect of Pd and Cu co-catalyst on the charge carrier trapping, recombination and transfer during photocatalytic hydrogen evolution over WO_3–TiO_2 heterojunction. J Mater Sci 55:16641–16658. https://doi.org/10.1007/s10853-020-05188-z
47. Mahmoud MHH, Ismail AA, Sanad MMS (2012) Developing a cost effective synthesis of active iron oxide doped titania photocatalysts loaded with palladium, platinum or silver nanoparticles. Chem Eng J 187:96–103. https://doi.org/10.1016/j.cej.2012.01.105
48. Chuaicham C, Pawar RR, Karthikeyan S, Ohtani B, Sasaki K (2020) Fabrication and characterization of ternary sepiolite/g-C_3N_4/Pd composites for improvement of photocatalytic degradation of ciprofloxacin under visible light irradiation. J Colloid Interface Sci 577:397–405. https://doi.org/10.1016/j.jcis.2020.05.064
49. Peng L, Xie T, Lu Y, Fan H, Wang D (2010) Synthesis, photoelectric properties and photocatalytic activity of the Fe_2O_3/TiO_2 heterogeneous photocatalysts. Phys Chem Chem Phys 12:8033–8041. https://doi.org/10.1039/c002460k
50. Liu C, Tong R, Xu Z, Kuang Q, Xie Z, Zheng L (2016) Efficiently enhancing the photocatalytic activity of faceted TiO_2 nanocrystals by selectively loading a-Fe_2O_3 and Pt co-catalysts. RSC Adv 6:29794–29801. https://doi.org/10.1039/c6ra04552a
51. Khasawneh OFS, Palaniandy P, Palaniandy P, Ahmadipour M, Mohammadi H, Bin HMR (2021) Removal of acetaminophen using Fe_2O_3-TiO_2 nanocomposites by photocatalysis under simulated solar irradiation: optimization study. J Environ Chem Eng 9:104921. https://doi.org/10.1016/j.jece.2020.104921
52. Cao Z, Qin M, Gu Y, Jia B, Chen P, Qu X (2016) Synthesis and characterization of Sn-doped hematite as visible light photocatalyst. Mater Res Bull 77:41–47. https://doi.org/10.1016/j.materresbull.2016.01.004
53. Topcu S, Jodhani G, Gouma PI (2016) Optimized nanostructured TiO_2 photocatalysts. Front Mater 3:1–9. https://doi.org/10.3389/fmats.2016.00035
54. Duo F, Wang Y, Mao X et al (2015) A $BiPO_4$/BiOCl heterojunction photocatalyst with enhanced electron hole separation and excellent photocatalytic performance. Appl Surf Sci 340:35–42. https://doi.org/10.1016/j.apsusc.2015.02.175
55. Zolfaghari P, Khaledian HR, Aliasgharlou N, Khorram S, Karimi A, Khataee A (2019) Facile surface modification of immobilized rutile nanoparticles by non-thermal glow discharge plasma: effect of treatment gases on photocatalytic process. Appl Surf Sci 490:266–277. https://doi.org/10.1016/j.apsusc.2019.06.077
56. Wang B, Li C, Cui H, Zhang J, Zhai J, Li Q (2013) Fabrication and enhanced visible-light photocatalytic activity of Pt-deposited TiO_2 hollow nanospheres. Chem Eng J 223:592–603. https://doi.org/10.1016/j.cej.2013.03.052
57. Bootluck W, Chittrakarn T, Techato K, Khongnakorn W (2021) Modification of surface α-Fe_2O_3/TiO_2 photocatalyst nanocomposite with enhanced photocatalytic activity by Ar gas plasma treatment for hydrogen evolution. J Environ Chem Eng 9:105660. https://doi.org/10.1016/j.jece.2021.105660
58. Ren D, Zhang W, Ding Y, Shen R, Jiang Z, Lu X, Li X (2020) In situ fabrication of robust cocatalyst-free CdS/g-C_3N_4 2D–2D step-scheme heterojunctions for highly active H_2 evolution. Sol RRL 4:1–11. https://doi.org/10.1002/solr.201900423
59. Haider Z, Kang YS (2014) Facile preparation of hierarchical TiO_2 nano structures: growth mechanism and enhanced photocatalytic H_2 production from water splitting using methanol as a sacrificial

reagent. ACS Appl Mater Interfaces 6:10342–10352. https://doi.org/10.1021/am501796m
60. Jiang Q, Li I, Bi J, Liang S, Liu M (2017) Design and synthesis of TiO_2 hollow spheres with spatially separated dual cocatalysts for efficient photocatalytic hydrogen production. Nanomaterials 7:24. https://doi.org/10.3390/nano7020024
61. Wu J, Lu S, Ge D, Zhang L, Chen W, Gu H (2016) Photocatalytic properties of Pd/TiO_2 nanosheets for hydrogen evolution from water splitting. RSC Adv 6:67502–67508. https://doi.org/10.1039/c6ra10408h
62. Liao CH, Huang CW, Wu JCS (2012) Hydrogen production from semiconductor-based photocatalysis via water splitting. Catalysts 2:490–516. https://doi.org/10.3390/catal2040490
63. Bhoi YP, Fang F, Zhou X, Li Y, Sun X, Wang J, Huang W (2020) Single step combustion synthesis of novel Fe_2TiO_5/α-Fe_2O_3/TiO_2 ternary photocatalyst with combined double type-II cascade charge migration processes and efficient photocatalytic activity. Appl Surf Sci 525:146571. https://doi.org/10.1016/j.apsusc.2020.146571
64. Mei Q, Zhang F, Wang N, Yang Y, Wu R, Wang W (2019) TiO_2/Fe_2O_3 heterostructures with enhanced photocatalytic reduction of Cr(vi) under visible light irradiation. RSC Adv 9:22764–22771. https://doi.org/10.1039/c9ra03531a
65. Lv YR, Liu CJ, He RK, Li X, Xu YH (2019) $BiVO_4$/TiO_2 heterojunction with enhanced photocatalytic activities and photoelectochemistry performances under visible light illumination. Mater Res Bull 117:35–40. https://doi.org/10.1016/j.materresbull.2019.04.032
66. Sing KSW, Williams RT (2004) Physisorption hysteresis loops and the characterization of nanoporous materials. Adsorpt Sci Technol 22:773–782. https://doi.org/10.1260/0263617053499032
67. Mohamed RM, Kadi MW, Ismail AA (2020) A Facile synthesis of mesoporous α-Fe_2O_3/TiO_2 nanocomposites for hydrogen evolution under visible light. Ceram Int 46:15604–15612. https://doi.org/10.1016/j.ceramint.2020.03.107
68. Dai X, Lu G, Hu Y, Xie X, Wang X, Sun J (2019) Reversible redox behavior of Fe_2O_3 /TiO_2 composites in the gaseous photodegradation process. Ceram Int 45:13187–13192. https://doi.org/10.1016/j.ceramint.2019.03.255
69. Fang X, Lu G, Mahmood A, Tang Z, Liu Z, Ln Z, Wang Y, Jing S (2020) A novel ternary Mica/TiO_2/Fe_2O_3 composite pearlescent pigment for the photocatalytic degradation of acetaldehyde. J Photochem Photobiol A Chem 400:112617. https://doi.org/10.1016/j.jphotochem.2020.112617
70. An M, Li L, Cao Y, Ma F, Liu D, Gu F (2019) Coral reef-like Pt/TiO_2-ZrO_2 porous composites for enhanced photocatalytic hydrogen production performance. Mol Catal 475:110482. https://doi.org/10.1016/j.mcat.2019.110482
71. Zhou W, Fu H, Pan K, Tian C, Qu Y, Lu P, Sun CC (2008) Mesoporous TiO_2/α-Fe_2O_3: bifunctional composites for effective elimination of arsenite contamination through simultaneous photocatalytic oxidation and adsorption. J Phys Chem C 112:19584–19589. https://doi.org/10.1021/jp806594m
72. Cheng Y, Guo H, Wang Y, Zhao Y, Li Y, Liu L, Hg Li, Duan H (2018) Low cost fabrication of highly sensitive ethanol sensor based on Pd-doped α-Fe_2O_3 porous nanotubes. Mater Res Bull 105:21–27. https://doi.org/10.1016/j.materresbull.2018.04.025
73. Zhang X, Lei L (2008) Preparation of photocatalytic Fe_2O_3 -TiO_2 coatings in one step by metal organic chemical vapor deposition. Appl Surf Sci 254:2406–2412. https://doi.org/10.1016/j.apsusc.2007.09.067
74. Pham MH, Dinh CT, Vuong GT, Ta ND, Do TO (2014) Visible light induced hydrogen generation using a hollow photocatalyst with two cocatalysts separated on two surface sides. Phys Chem Chem Phys 16:5937–5941. https://doi.org/10.1039/c3cp54629b
75. Gao J, Jiang R, Wang J, Wang B, Li K, Pi K, Li Y, Zhang X (2011) Sonocatalytic performance of Er^{3+}:$YAlO_3$/TiO_2-Fe_2O_3 in organic dye degradation. Chem Eng J 168:1041–1048. https://doi.org/10.1016/j.cej.2011.01.079
76. Wang Y, Yu J, Li Q (2014) Microwave-assisted hydrothermal synthesis of graphene based Au – TiO_2 photocatalysts for e ffi cient visible-light hydrogen production. J Mater Chem. https://doi.org/10.1039/c3ta14908k
77. Sayed FN, Sasikala R, Jayakumar OD, Rao R, Betty CA, Chokkalingam A, Kadam RM, Jagannath J, Bharadwaj SR, Vinu A, Tyagi AK (2014) Photocatalytic hydrogen generation from water using a hybrid of graphene nanoplatelets and self doped TiO_2-Pd. RSC Adv 4:13469–13476. https://doi.org/10.1039/c3ra47974a
78. Xu Q, Lg Z, Cheng B, Fan Ji YuJ (2020) S-scheme heterojunction photocatalyst. Chem 6:1543–1559. https://doi.org/10.1016/j.chempr.2020.06.010
79. Liu J, Yang S, Wu W, Tian Q, Sn C, Dai Z, Ren F, Xiao X, Jiang C (2015) 3D flowerlike α-Fe_2O_3@TiO_2 core-shell nanostructures: general synthesis and enhanced photocatalytic performance. ACS Sustain Chem Eng 3:2975–2984. https://doi.org/10.1021/acssuschemeng.5b00956
80. Ge H, Xu F, Cheng B, Yu J, Ho W (2019) S-scheme heterojunction TiO_2/CdS nanocomposite nanofiber as H_2-production photocatalyst. ChemCatChem 11:6301–6309. https://doi.org/10.1002/cctc.201901486
81. Xie MY, Su KY, Peng XY, Wu RJ, Chavali M, Chang WC (2017) Hydrogen production by photocatalytic water-splitting on Pt-doped TiO_2–ZnO under visible light. J Taiwan Inst Chem Eng 70:161–167. https://doi.org/10.1016/j.jtice.2016.10.034
82. Xu Q, Ma D, Yang S, Tian Z, Cheng B, Fan J (2019) Novel g-C_3N_4/g-C_3N_4 S-scheme isotype heterojunction for improved photocatalytic hydrogen generation. Appl Surf Sci 495:143555. https://doi.org/10.1016/j.apsusc.2019.143555
83. Zhang H, Liu F, Wu H, Cao X, Sun J, Lei W (2017) In situ synthesis of g-C_3N_4/TiO_2 heterostructures with enhanced photocatalytic hydrogen evolution under visible light. RSC Adv 7:40327–40333. https://doi.org/10.1039/c7ra06786k
84. Chem JM, Martha S, Das DP, Biswal N, Parida KM (2012) Photocatalyst : enhanced hydrogen production and phenol degradation. J Mater Chem 5:10695–10703. https://doi.org/10.1039/c2jm30462g

Authors and Affiliations

Weerapong Bootluck[1,2] · Thawat Chittrakarn[2] · Kuaanan Techato[1,3] · Panitan Jutaporn[4] · Watsa Khongnakorn[2,5]

[1] Faculty of Environmental Management, Prince of Songkla University, Hat Yai 90110, Songkhla, Thailand

[2] Center of Excellence in Membrane Science and Technology, Prince of Songkla University, Hat Yai 90110, Songkhla, Thailand

[3] PSU Energy Systems Research Institute, Prince of Songkla University, Hat Yai 90110, Songkhla, Thailand

[4] Research Center for Environmental and Hazardous Substance Management (EHSM), Department of Environmental Engineering, Faculty of Engineering, Khon Kaen University, Khon Kaen 40002, Thailand

[5] Department of Civil and Environmental Engineering, Faculty of Engineering, Prince of Songkla University, Hat Yai 90110, Songkhla, Thailand

CHAPTER 3

This chapter presents the modification of heterojunction photocatalyst of α-Fe_2O_3/TiO_2 nanocomposite by Ar-plasma treatment for hydrogen evolution. The α-Fe_2O_3/TiO_2 has obtained a characterization of the crystal structure, optical properties, bandgap energy, surface morphology, elemental composition and charge carrying capacity of the photocatalyst nanocomposite was investigated. Finally, the performance of α-Fe_2O_3/TiO_2 for the H_2 production and photocatalyst stability was investigated. This article has been published in the title of “Modification of surface α-Fe_2O_3/TiO_2 photocatalyst nanocomposite with enhanced photocatalytic activity by Ar gas plasma treatment for hydrogen evolution” in the Journal of Environmental Chemical Engineering.

PAPER II

Modification of surface α-Fe_2O_3/TiO_2 photocatalyst nanocomposite with enhanced photocatalytic activity by Ar gas plasma treatment for hydrogen evolution.

Journal of Environmental Chemical Engineering, 9 (4), 105660.
https://doi.org/10.1016/j.jece.2021.105660

Journal of Environmental Chemical Engineering 9 (2021) 105660

Contents lists available at ScienceDirect

Journal of Environmental Chemical Engineering

journal homepage: www.elsevier.com/locate/jece

Modification of surface α-Fe_2O_3/TiO_2 photocatalyst nanocomposite with enhanced photocatalytic activity by Ar gas plasma treatment for hydrogen evolution

Weerapong Bootluck [a,b], Thawat Chittrakarn [b], Kuaanan Techato [a,c], Watsa Khongnakorn [b,d,*]

[a] Faculty of Environmental Management, Prince of Songkla University, Hat Yai, Songkhla 90110, Thailand
[b] Center of Excellence in Membrane Science and Technology, Prince of Songkla University, Hat Yai, Songkhla 90110, Thailand
[c] PSU Energy Systems Research Institute, Prince of Songkla University, Hat Yai, Songkhla 90110, Thailand
[d] Department of Civil and Environmental Engineering, Faculty of Engineering, Prince of Songkla University, Hat Yai, Songkhla 90110, Thailand

ARTICLE INFO

Editor: Dr. GL Dotto

Keywords:
Photocatalytic
α-Fe_2O_3/TiO_2
Hydrogen evolution
Ar-plasma treatment

ABSTRACT

In this work, hematite (α-Fe_2O_3) deposited on anatase TiO_2 was modified by plasma treatment and studied. α-Fe_2O_3/TiO_2 was successfully synthesized using sol-gel precipitation methods and the surface was modified by argon (Ar) gas plasma treatment to increase photocatalyst nanocomposite activity. The effect of Ar-plasma treatment times from 5 to 20 min at DC glow discharge powers of 50 watts was investigated. The crystal structures, surface morphology, optical properties were characterization by using X-ray Diffractometry (XRD), scanning electron microscopy (SEM), transmission electron microscopy (TEM), atomic force microscopy (AFM), UV–vis spectrometry (UV–Vis), X-ray photoelectron spectroscopy (XPS), photoluminescence spectroscopy (PL) and electrochemical impedance spectroscopy (EIS). After plasma treatment, the crystalline phase of TiO_2 form changed from pure anatase to a mixture of anatase and rutile phases. The particle size was reduced from 25 to 20 nm. The band gap energy decreased from approximately 2.18 eV to 1.84 eV and exhibited a wider absorption edge under visible light irradiation (400–700 nm). Ar-plasma modification of the surface showed the attribution of oxygen vacancies and Ti^{3+}. The plasma treatment improved the heterojunction photocatalyst to enhance the photocatalytic activity under visible light for H_2 evolution. The best photocatalytic activity for H_2 evolution rate was obtained at 1.25 mmol h^{-1} for α-Fe_2O_3/TiO_2-10 photocatalyst compared to α-Fe_2O_3/TiO_2-untreated (0.13 mmol h^{-1}). The plasma treatment on photocatalyst materials showed long-term stability and excellent separation of the photogenerated charge carriers.

1. Introduction

Currently, energy sources from fossil fuels are limited and cause environmental pollution, which is a problem that can be solved by renewable energy [1–5]. Renewable energy sources from both solar and wind energy are considered a promising technology for cheap and unlimited energy from natural resources [6–8]. Hydrogen (H_2) is an ideal solution to provide energy in the future because of its high efficiency and cleanliness [6,9]. There are several methods for H_2 production from solar light, including photoelectrochemical [6], photocatalysis [5], photoelectrolysis [6] and photobiological [10]. Photocatalytic splitting of water was proposed to produce H_2 under solar light irradiation because it is a sustainable energy source that is environmentally friendly [11].

Photocatalytic water splitting for H_2 evolution was reported by using titanium dioxide (TiO_2) as a semiconductor material.TiO_2 nanoparticle semiconductor materials have been widely studied in photocatalysis because of high stability, specific morphology and low toxicity [12,13]. However, anatase TiO_2 phase has a wide band gap (3.2 eV) of photocatalytic activity and is active only under UV light irradiation with fast recombination of electron and hole pair (e^-,h^+) [3,14,15]. In general, of the three crystalline phases of TiO_2 (anatase, rutile and brookite), anatase phase is the most used as a photocatalyst due to less recombination of the electron-hole pair when compared with other phases [16–18]. The crystalline structure of mixed phase anatase TiO_2 (3.2 eV) and rutile TiO_2 (3.02 eV) [19] and the commercial Degussa P25 commonly show higher performance of photocatalytic activity [20]. It has reduced band gap energy, increased absorption under visible light

* Corresponding author at: Center of Excellence in Membrane Science and Technology, Prince of Songkla University, Hat Yai, Songkhla 90110, Thailand.
E-mail address: watsa.k@psu.ac.th (W. Khongnakorn).

https://doi.org/10.1016/j.jece.2021.105660
Received 16 January 2021; Received in revised form 13 April 2021; Accepted 8 May 2021
Available online 14 May 2021

and enhanced photoactivity.

Photocatalytic activity of TiO_2-based photocatalysts can gain enhanced absorbance of visible light and increased separation of the electron-hole pair with metal deposition as a light-scattering material, such as TiO_2/WO_3 [21], TiO_2/ZnO [22], TiO_2/SnO_2 [23], Cu_2O/TiO_2 [24] and TiO_2/Fe_2O_3 [25], etc. For illustration, Lee et al. [23] found that the composite TiO_2/SnO_2 exhibited high visible light harvesting and could be applied as a photocatalyst for H_2 evolution. Yan et al. [24], studied the composite TiO_2/Cu_2O and found a high efficiency in charge transfer of electron hole rate and a high H_2 evolution rate (16.25 mmol h^{-1} g^{-1}).

Heterojunction nanocomposites for photocatalysis are desired for their higher efficacy, reuse ability, environmental friendliness, high stability and low cost. Increased photocatalyst efficiency is currently in focus for the application of water splitting and wastewater treatment. One of the noble metals that can be deposited over TiO_2 is hematite (α-Fe_2O_3), a metal oxide with a narrow bandgap of about 2.0–2.2 eV [26]. It seems to be a suitable semiconductor photocatalyst for H_2 evolution, with efficiency harvesting in the solar spectrum (43%), excellent stability, non-toxic and is cost-effective [27–30]. Several studies (Madhumitha et al. [27], Fu et al. [31], Mohamed et al. [32], Lu et al. [33], Zhu et al. [34]) have demonstreted that α-Fe_2O_3 deposition on TiO_2 nanoparticles have effective charge separation, enhanced visible light absorption and enhanced photocatalytic activity for H_2 evolution. The methods that have been reported for the fabrication of photocatalytic α-Fe_2O_3/TiO_2 nanocomposite heterojunction include sol-gel [35], hydrothermal and impregnation methods [36,37]. To improve the photocatalytic activity of TiO_2-based photocatalysts, various fabrication methods have been tried, but remain a challenge. The drawback of α-Fe_2O_3 is the limited performance and high recombination rate of the photogenerated electrons and hole [38,39].

The plasma process was reported to modify the surface properties of photocatalysts, where the presence of highly stable Ti^{3+} [40–42] and oxygen vacancy could improve the performance of photogenerated charge carriers [40,43,44]. The advantage of plasma treatment is low energy consumption and not requiring any toxic chemicals [45]. In previous studies, Kong et al. [46] studied Ar plasma treatment could cause oxygen vacancy defects over a TiO_2/GO heterojunction that improved photocatalyst activity and separation of the photogenerated electron-hole pair for H_2 evolution. Xing et al. [47] found that Ar plasma modification of surface Pt/g-C_3N_4 nanosheets can improve charge transfer of photogenerated performance for enhanced H_2 evolution in photocatalytic activity. So Ar-plasma can be used to produce oxygen vacancy defects in a metal oxide, one of the most stable methods of creating Ti^{3+} in TiO_2. For example, Sun et al. [48] modified the surface of $TiO_2/CoFe_2O_4$ using Ar-plasma and showed that changing uniform TiO_2 to anatase and rutile phase produced oxygen vacancy defects on the surface which improved the photocatalytic activity. Kawakami et al. [49] have modified anatase TiO_2 by Ar gas, they found the mix of anatase and rutile phase increased with plasma treatment time. Plasma methods do not require high temperatures to modify the structure of TiO_2 anatase to mixed anatase and rutile phase, which is a benefit compared to annealing methods that typically use calcination at temperatures of 450–900 °C for at least 2 h [50]. Therefore, Ar plasma treatment can be used to improved properties of TiO_2 crystalline structure, alter the phase to mixed anatase and rutile phase and enhance photocatalytic activity with less recombination of electron-hole pairs.

The photocatalytic activity of α-Fe_2O_3/TiO_2 nanocomposite for H_2 evolution by Ar-plasma treatment have not been previously reported. In this work, α-Fe_2O_3 was loaded onto TiO_2 by using the sol-gel precipitation methods and the surface of α-Fe_2O_3/TiO_2 was modified by Ar-treatment at several exposure times (5–20 min) to improve the photocatalytic activity. The crystal structure, optical properties, bandgap energy, surface morphology, elemental composition and charge carrying capacity of the photocatalyst nanocomposite was investigated. Finally, the performance of α-Fe_2O_3/TiO_2 for the H_2 evolution and photocatalyst stability was investigated.

2. Material and methods

2.1. Preparation of TiO_2

TiO_2 nanoparticle was synthesized according to previous studies by Peng et al. [51]. Titanium (IV) butoxide (Ti $(OC(CH_3)_3)_4$, Sigma-Aldrich, USA), 3 mL, was mixed with ethylene glycol (Loba Chemie, India), 30 mL, in a bottle flask. The solution of pure TiO_2 was treated at 180 °C with magnetic stirring for 2 hrs. The white precipitate of TiO_2 was centrifuged at 5000 rpm (Force 7, Denver Instrument, USA) and washed with ethanol (EtOH, Ar 99.9%, RCI Labscan, Thailand) and deionized water several time. Finally, the sample was calcined at 450 °C for 2 hrs to a stable pure TiO_2 dry powder.

2.2. Preparation of α-Fe_2O_3/TiO_2 on Ti substrate

The synthesis of α-Fe_2O_3 on TiO_2 nanocomposite photocatalyst is show in Fig. 1. Firstly, pure TiO_2 powder (1.5 g) from Section 2.1 and 30 mL of iron (III) nitrate nonahydrate Fe $(NO_3)_3 \bullet 9H_2O$, (Ajax Finecem, Australia) 50 wt% was mixed in ethanol under magnetic stirring for 30 min and evaporated at 50 °C.

To deposit α-Fe_2O_3/TiO_2 nanocomposite on Ti substrate, α-Fe_2O_3/TiO_2 (1.5 g) powder was dispersed in 50 mL of DI water. After that, 0.06 g Polyethylene glycol (PEG, Mw 6000, Ajax Finecem, Australia) was dropped into the above solution and mixed under stirring for 30 min. The coating was formed on the Ti (3 × 5 cm) substrate by the dip-coating method. Finally, Ti substrates were immersed in the aqueous solution for 10 min and then dried in a vacuum oven at 120 °C for 30 min

2.3. Plasma procedure

The plasma treatment process used Argon (Ar) (purity 99.9%; flow rate, 50 sccm) gas flow in a plasma reactor [52]. A DC power supply of 50 W was used to generate plasma discharges. Plasma treatment exposure times were 5, 10, 15 and 20 min to produce photocatalytic nanocomposite materials, referred to as α-Fe_2O_3/TiO_2-5, α-$Fe_2O_3TiO_2$-10, α-Fe_2O_3/TiO_2-15 and α-Fe_2O_3/TiO_2-20, respectively. A schematic illustration of the plasma procedure is shown in Fig. 2.

2.4. Characterization of materials

The surface morphology was measured by a scanning electron microscope (SEM, Quanta 400, Thermo Fisher Scientific, USA). Morphology was determined by Transmission electron microscopy (TEM, Tecnai G2 20 S-TWIN 200 KV, FEI, USA). The chemical component surface was analyzed by X-ray photoelectron spectroscopy (XPS, AXIS Ultra DLD, Krotos Analytical, UK). The crystal structure was determined using an X-ray Diffractometer (XRD, X' Pert MPD, PHILIPS, Netherlands) with a Cu Kα source ($\lambda = 0.1540$ Å) scanning at the 2θ range from 20° to 80°. The band gap was calculated by a UV–vis spectrometer (UV-Shimadzu, Japan). The surface roughness was measured using an Atomic Force Microscope (AFM, Nanosurf easy Scan2, Switzerland). The electron-hole pair recombination rate of the photocatalyst was measured by a photoluminescence spectrometer (PL; Avantes AvaSpec-2048, Netherlands) at an excitation wavelength 590 nm.

2.5. Electrochemical impedance spectroscopy (EIS)

The electrochemical impedance spectroscopy (EIS) was performed by using a Potentiostat/Galvanostats (PGSTAT302N, Metrohm, Autolab, Netherland) workstation with three electrode cells. The fluorine-doped tin oxide (FTO) electrode performed deposition with the photocatalyst

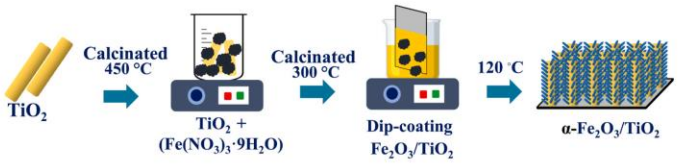

Fig. 1. The synthesis of photocatalyst of the α-Fe_2O_3 on TiO_2 nanocomposite.

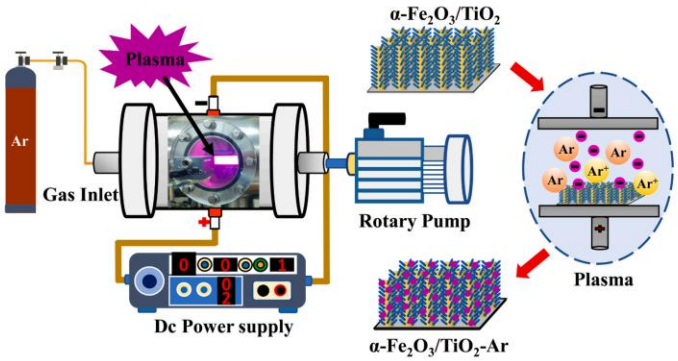

Fig. 2. Schematic illustration of the plasma-treated on α-Fe_2O_3/TiO_2 photocatalytic nanocomposite.

samples, platinum wire and a Ag/AgCl electrode was used as the counter electrode and reference electrode, respectively [53]. EIS was performed at voltage amplitude of 10 mV with a frequency range of 0.01–1,000, 000 Hz with 0.5 M Na_2SO_4 aqueous solution as the electrolyte [43]. Fabrication of photocatalyst samples for the working electrodes were prepared as follows: 0.05 g of photocatalyst sample was mixed with 1 mL ethanol for 20 min and deposited on 1 × 2 cm^2 FTO glass electrodes and dried at 80 °C for 6 h. The light source was a 250 W mercury lamp (12750 lumens, Philips, NPL-N).

2.6. H_2 evolution

The photocatalytic activity reactor was set up in a plexiglass cell with a volume 500 mL. A mercury lamp 250 W (12750 lumens, Philips, NPL-N) was used as a visible light source positioned 15 cm^2 away from the plexiglass on the opposite side to the photocatalytic reactor. The photocatalyst samples of TiO_2, α-Fe_2O_3/TiO_2 and plasma-treated α-Fe_2O_3/TiO_2 (α-Fe_2O_3/TiO_2-5, α-$Fe_2O_3TiO_2$-10, α-Fe_2O_3/TiO_2-15 and α-Fe_2O_3/TiO_2-20) were put into the photocatalyst reactor with a sacrificial agent solution in methanol: water (30: 70 v/v). Before photocatalyst testing in the photocatalytic reactor, argon (Ar purity 99.99%) gas was flowed into the reactor for 30 min to completely remove air. The amount of H_2 concentration was analyzed by gas chromatography (GC; Hewlett Packard, HP 6890, USA) equipped with a thermal conductivity detector (TCD). For the analysis, gas was injected through 5 Å molecular sieve stainless steel columns and helium (He) gas was used as a carrier gas. The concentration of hydrogen was calculated using standard curve calibration. The H_2 evolution rate was calculated following Heider and Kang [54]. The recycling stability of the photocatalyst reaction was tested for each sample and repeated five times for each cycle [55]. Ferric ion and titanium leaching of the photocatalytic reaction after used for each recycle time was determined by an inductively coupled plasma optical emission spectrometry (ICP-OES, Avio 500, Perkin Elmer, USA) [56].

3. Results and discussion

3.1. α-Fe_2O_3/TiO_2 photocatalyst nanocomposite characteristic

XRD analysis of the crystalline characteristics of the plasma modified α-Fe_2O_3 deposited on anatase TiO_2 nanoparticle shows the anatase TiO_2 as representative diffraction peaks at 2θ = 25.3°, 37.8°, 48.14°, 53.9° and 54.1° (Fig. 3), which is attributed to the (101), (004), (200), (211), (204) and (116) (JCDPS No. 21-1272), respectively [39,51]. While the hematite diffraction peaks appearing at 2θ = 24.1°, 33.1°, 35.6°, 40.8°, 49.4°, 54.1° 62.4° and 64.0° can be attributed to the (012), (104), (110),

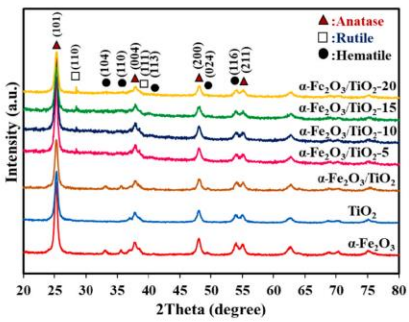

Fig. 3. XRD patterns of TiO_2, α-Fe_2O_3, α-Fe_2O_3/TiO_2, α-Fe_2O_3/TiO_2-5, α-Fe_2O_3/TiO_2-10, α-Fe_2O_3/TiO_2-15 and α-Fe_2O_3/TiO_2-20, at different 2Theta angles.

(024), (116), (214) and (300) lattice plane of α-Fe_2O_3 (JCPDS 73-2234), respectively. It can be seen that Ar-plasma treatment modified the surface anatase TiO_2 to rutile phase with the amount correlating to exposure time, the result showed a new small peak of rutile phase TiO_2 at $2\theta = 28.5^{\circ}$ corresponding to the (110) [48]. Also, XRD showed a modified photocatalytic surface, it was observed that a mixture of anatase and rutile phase were presented, which is in agreement with a previous study by Sun et al. [48]. Kawakami et al. [49] also reported a mix of anatase and rutile phase correlating to the Ar-plasma etching time.

The Ar-plasma treatment modifies the surface α-Fe_2O_3/TiO_2 by changing pure anatase TiO_2 to a mix of anatase and rutile phase, and this can be attributed to the energetic electrons in the plasma [48]. Also, since the lattice structure and ionic radius of Fe^{3+} and Ti^{4+} are similar, the iron could diffuse into the TiO_2 lattice converting the junction from anatase to rutile phase [48].

The average crystallite size of TiO_2, α-Fe_2O_3, α-Fe_2O_3/TiO_2 nanocomposite and α-Fe_2O_3/TiO_2 with various plasma treatment times ranged from 19.01 ± 4.95–23.50 ± 6.61 (Table 1). The average crystallite size was calculated from the XRD peak using the Debye-Scherrer equation as follows [57]:

$$d = \frac{k\lambda}{\beta cos\theta} \quad (1)$$

where d is the crystallite size (nm), λ is the X-ray wavelength (nm), k is a constant related to the crystallite shape and normally taken as 0.89, β is the peak width at half maximum (FWHM) of the XRD peak and θ is the diffraction angle [57]. The crystallite average size of TiO_2, α-Fe_2O_3 and α-Fe_2O_3/TiO_2 nanocomposite was 19.01 ± 4.95 nm, 21.78 ± 1.74 nm and 23.50 ± 6.61 nm, respectively. It can be seen that after plasma treatment of α-Fe_2O_3/TiO_2-5, α-$Fe_2O_3TiO_2$-10, α-Fe_2O_3/TiO_2-15 and α-Fe_2O_3/TiO_2-20, the crystalline size was reduced from 23.50 ± 6.61 nm to 20.13 ± 2.63 nm. This may be attributed to effect of Ar plasma treatment on the surface of the sample. The smaller crystalline size resulted in a higher photocatalytic activity with a wider absorption of visible light irradiation. The crystallinity of α-Fe_2O_3/TiO_2-untreated photocatalyst was 92.55%. After plasma modification on the surface, it can be seen that the crystallinity was 78.23–83.45% for the α-Fe_2O_3/TiO_2, α-Fe_2O_3/TiO_2-5, α-$Fe_2O_3TiO_2$-10, α-Fe_2O_3/TiO_2-15 and α-Fe_2O_3/TiO_2-20.

The UV–vis diffuse reflectance spectroscopy (DSR) absorption spectrum of TiO_2, α-Fe_2O_3 and α-Fe_2O_3/TiO_2 was recorded within the range of 200–800 nm, as shown in Fig. 4. It can be observed that TiO_2 shows the absorption of only UV light (420 nm), while α-Fe_2O_3 absorbed over the visible region (580 nm). It was observed that the heterojunction of α-Fe_2O_3/TiO_2 photocatalyst shows wide absorption of UV–visible light. After plasma treatment, the absorption edge of the α-Fe_2O_3/TiO_2 shows significantly enhanced absorption over the visible light region of 400–700 nm. The stroger absorption edge of the plasma treated

Table 1
The average crystallite size, crystallinity, and band gap energy of various samples.

Sample	Average crystallite size (nm)	Crystallinity (%)	Band Gap Energy (eV)
TiO_2	19.01 ± 4.95	95.01	3.16
α-Fe_2O_3	21.78 ± 1.74	65.82	2.02
α- Fe_2O_3/TiO_2	23.50 ± 6.61	92.55	2.18
α-Fe_2O_3/TiO_2-5	21.76 ± 7.82	82.63	1.88
α-Fe_2O_3/TiO_2-10	21.50 ± 3.76	78.23	1.84
α-Fe_2O_3/TiO_2-15	21.74 ± 5.31	78.99	1.90
α-Fe_2O_3/TiO_2-20	20.13 ± 2.63	83.45	1.86

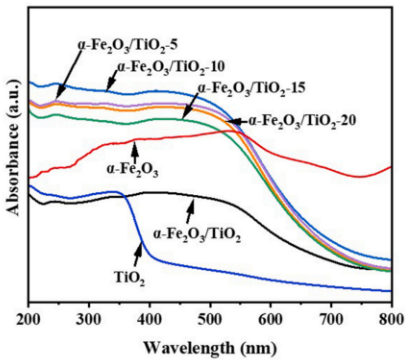

Fig. 4. UV–Vis absorption spectra of TiO_2, α-Fe_2O_3, α-Fe_2O_3/TiO_2, α-Fe_2O_3/TiO_2-5, α-Fe_2O_3/TiO_2-10, α-Fe_2O_3/TiO_2-15 and α-Fe_2O_3/TiO_2-20.

α-Fe_2O_3/TiO_2-5, α-$Fe_2O_3TiO_2$-10, α-Fe_2O_3/TiO_2-15 and α-Fe_2O_3/TiO_2-20 increases with increasing Ar-plasma treatment time of α-Fe_2O_3/TiO_2.

The optical band gap energy of the TiO_2 and α-Fe_2O_3 nanoparticles was calculated by Tac'c plot equation following [58]:

$$\alpha h\nu = A\,(h\nu\text{-}E_g)^{n/2} \quad (2)$$

where α is the absorbance, h is Planck's constant, ν is the light frequency, A is a constant, E_g is the band gap energy and the value of n depends on the type of optical transition [58]. Optical band gap energy of the sample is shown in Table 1 and Fig. 5. The TiO_2 and α-Fe_2O_3 has band gap energy and was obtained at 3.16 eV and 2.02 eV, respectively. The band gap energy of photocatalyst α-Fe_2O_3/TiO_2 nanocomposite was found at 2.18 eV. Optical band gap energy of Ar-plasma treated photocatalyst were found to be 1.88, 1.84, 1.90 and 1.86 eV for α-Fe_2O_3/TiO_2-5, α-$Fe_2O_3TiO_2$-10, α-Fe_2O_3/TiO_2-15 and α-Fe_2O_3/TiO_2-20, respectively. From the above results, the band gap energy was reduced after plasma treatment from 2.18 eV to 1.84 eV. The reduced band gap energy shows improved photocatalytic activity with visible light after modification by Ar-plasma treatment. However, the optimum Ar plasma treatment time was 10 min to produce a band gap of 1.84 eV (α-Fe_2O_3/TiO_2-10).

Fig. 6 **(a)** shows the high-resolution XPS survey scan spectrum of the O 1s, Ti 2p and Fe 2p elements for both the α-Fe_2O_3/TiO_2 untreated and Ar-plasma treated. The high resolution of O 1s is presented in Fig S1, the O 1s spectrum displayed a lattice structure centered at 528.84 eV, which was attributed to the lattice oxygen in the oxides O [43]. The weak peak at 531.27 eV was attributed to the defect oxygen vacancies (-OH), and the binding peak at 532.29 was attributed to the presence of surface oxygen, which is mainly attributed to lattice oxygen combined with Fe^{3+} and Ti^{4+} [39]. Hence, it can be seen that after plasma treatment with Ar, contribution of the oxygen vacancies (OH) was increased with binding energy shifts from 532.29 eV to 531.80 eV. An additional binding peak at the binding energies of TiO_2 corresponds to Ti^{3+} [40]. In addition, the high-resolution XPS of Fe is shown in Fig. 6 **(b)**, the binding energies of Fe at 711.09 and 724.26 eV correspond to Fe $2p_{3/2}$ and Fe $2p_{1/2}$ of α-Fe_2O_3, and satellite peak at 718.2 eV (Fe^{3+} $2p_{3/2}$) corresponds to the Fe^{3+} ion state in α-Fe_2O_3 [26,43]. The XPS result shows that plasma treatment of increased the Fe by 0.79%. The high-resolution scan spectrum of Ti in Fig. 6 **(c)** shows four binding peaks at 458.58, 464.10, 464.21 and 465.38 eV corresponding to Ti^{3+} $2p_{3/2}$, $Ti^{4+}2p_{3/2}$, Ti^{3+} $2p_{1/2}$, and Ti^{4+} $2p_{3/2}$, respectively. The split between the Ti $2p^{3+}{}_{1/2}$ (5.9 eV), indicates the presence of Ti^{4+} in anatase TiO_2. The Ti $2p_{1/2}$ peak, at 458.58 eV, is due to the formation of the Fe-O-Ti bond of nanocomposite in the α-Fe_2O_3/TiO_2 [59]. All of the above results

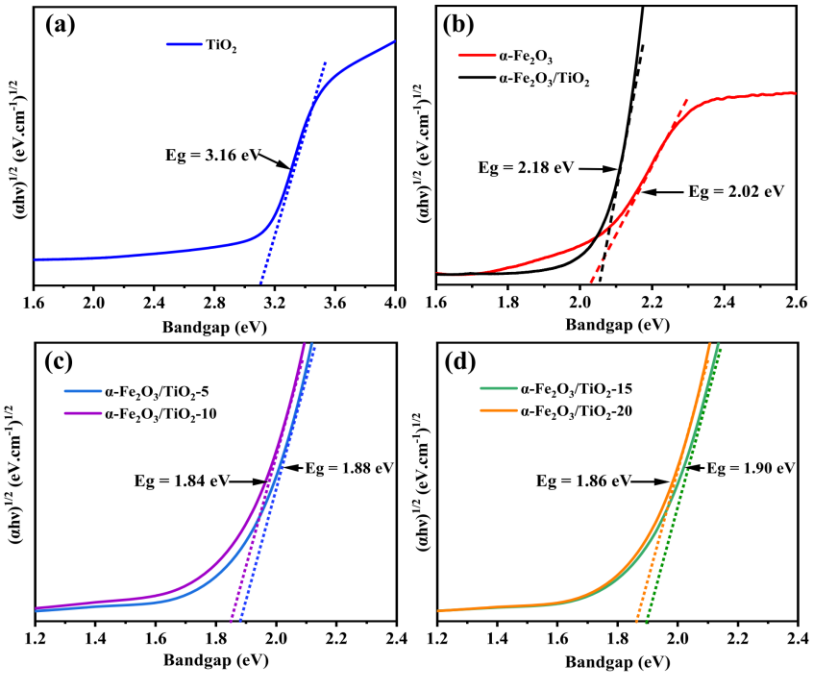

Fig. 5. Tach Plot of (a) TiO_2, (b) α-Fe_2O_3, α-Fe_2O_3/TiO_2, (c) α-Fe_2O_3/TiO_2-5, α-Fe_2O_3/TiO_2-10 and (d) α-Fe_2O_3/TiO_2-15, α-Fe_2O_3/TiO_2-20.

indicate that the plasma modification on heterojunctions of α-Fe_2O_3/-TiO_2 nanocomposite have been synthesised successfully.

The properties and calculated valence bands (VB) of TiO_2 and α-Fe_2O_3 were plotted from the XPS spectra of according to Bhoi et al. [60] and Naldoni et al. [61], as shown in Fig. 6 **(d)**. The VB position of TiO_2 and α-Fe_2O_3 were found to be 2.79 eV and 1.38 eV, respectively. Then the conduction band (CB) and band edge position of TiO_2 and α-Fe_2O_3 were calculated using the equation as follows [60]:

$$E_{CB} = E_{VB} - E_g \quad (3)$$

where E_{CB} and E_{VB} is the conduction band (CB) edge and valence band (VB) edge potential, respectively, and E_g is the band gap energy of the semiconductor calculated from optical absorption. The calculated CB position of TiO_2 and α-Fe_2O_3 was estimated to be − 0.27 eV and − 0.63 eV, respectively. The band position VB of α-Fe_2O_3 is higher than the TiO_2 band position. The CB band position α-Fe_2O_3 is higher than that of TiO_2 photocatalyst as shown in Table 2.

The PL spectra was used to investigate the recombination rate of the photogenerated electron hole-pair, presented in Fig. 7 **(a)**. The PL spectra of TiO_2 nanoparticle had higher intensity, showing a lower separation efficiency of electron-hole pair. The emission intensity of α-Fe_2O_3/TiO_2 nanocomposite was lower than that of pure TiO_2, indicating reduced recombination rate of the photogenerated electron-hole pair. The Ar- plasma treated surface of α-Fe_2O_3/TiO_2 nanocomposite had the lowest PL intensity, which means that the photogenerated charge carriers had high photocatalytic efficiency [62].

To confirm the charge transfer resistance, semicircle size in a Nyquist plot was investigated by EIS, shown in Fig. 7 **(b).** It was observed that the Nyquist impedance plots for TiO_2 had a larger semicircle than α-Fe_2O_3/TiO_2 or α-Fe_2O_3/TiO_2-10, indicating a higher charge transfer resistance. After modification by plasma treatment, α-Fe_2O_3/TiO_2-10 had the smallest semicircle in the Nyquist impedance plot, suggesting that the charge transfer resistance was decreased [63]. The charge transfer resistance was 2.93, 2.24, and 1.90 kΩ for TiO_2, α-Fe_2O_3/TiO_2 and α-Fe_2O_3/TiO_2-10, respectively. This result suggested that the plasma treatment of α-Fe_2O_3/TiO_2 reduced recombination rate of charge transfer, increased conductivity and allowed for rapid migration between the charge carrier interface [47]. It was demonstrated that plasma modification of photocatalyst surface reduced the charge transfer resistance due to enhanced performance of photocatalytic activity.

The surface SEM image of the TiO_2, α-Fe_2O_3/TiO_2, α-Fe_2O_3/TiO_2-5, α-$Fe_2O_3TiO_2$-10, α-Fe_2O_3/TiO_2-15 and α-Fe_2O_3/TiO_2-20 are shown in Fig. 8. The morphology of pure TiO_2 shows an average length of 5–7 μm and an average of diameter of 50–100 nm, as shown in Fig. 8 **(a)**. It was observed in the SEM image that α-Fe_2O_3/TiO_2 shows a rough surface, Fig. 8 **(b)**. While Fig. 8 **(c–f)** show that after Ar-plasma treatment, the spherical particles were slightly less densely packed on the surface with increasing Ar-plasma treatment time [43,64]. The conduct morphology of the photocatalytic activity of α-Fe_2O_3/TiO_2 was characterized using TEM, HR-TEM and SAED, as shown in Fig. 9 **(a–c).** It can be seen in the TEM image of the α-$Fe_2O_3TiO_2$ nanocomposite that the lattice spacing of 0.35 nm corresponds to the (101) plane of anatase TiO_2 and the lattice spacing of 0.25 nm corresponds to (110) plane of α-Fe_2O_3. The selected area electron diffraction (SAED) pattern is shown in Fig. 9 **(d)**, the SAED pattern formation shows (101), (004) and (200) for TiO_2 and (110), (104) and (116) for α-Fe_2O_3, confirming the polycrystalline structure

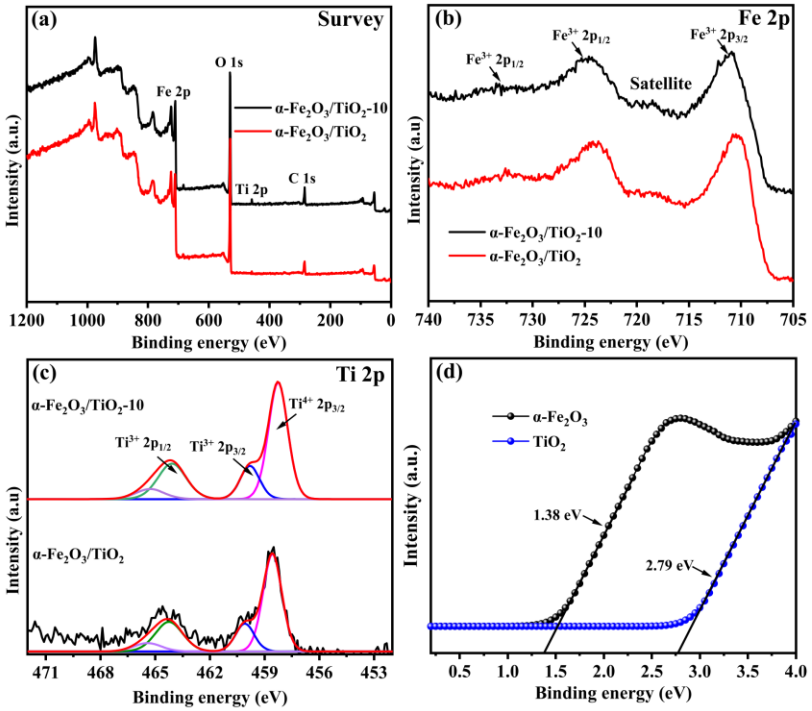

Fig. 6. XPS survey spectra patterns of (a) α-Fe_2O_3/TiO_2-10 XPS pattern (b) Fe2p, (c) Ti 2p, and (d) XPS valence band of α-Fe_2O_3 and TiO_2.

Table 2
The band gap, calculated valence band (VB) and conduction band (CB) position of TiO_2 and α-Fe_2O_3.

Sample	Band gap (eV)	E_{VB} (eV)	E_{CB} (eV)
TiO_2	3.16	2.79	-0.27
α-Fe_2O_3	2.02	1.38	-0.63

and successful synthesis of α-Fe_2O_3/TiO_2 nanocomposite, consistent with a report by Liu et al. [65].

The AFM was used to study the surface roughness of the α-Fe_2O_3/TiO_2 heterojunction photocatalyst as shown in Fig S2 **(a,b).** It can be seen that the surface roughness of the α-Fe_2O_3/TiO_2 photocatalyst is Ra = 46.71 nm and Ar-plasma treated is Ra = 44.87 nm. The AFM results revealed that plasma treatment of α-Fe_2O_3/TiO_2-10 decreased the surface roughness and increased homogeneity compared with untreated α-Fe_2O_3/TiO_2 photocatalyst nanocomposite [42].

The EDS mapping of plasma-treated heterojunction α-Fe_2O_3/TiO_2 photocatalytic nanocomposite confirmed typical deposited elements of O, Ti and Fe presented in Fig. S3 **(a).** The survey mapping of α-Fe_2O_3/TiO_2 after Ar plasma treatment shows the elements of O, Fe and Ti on the surface. It demonstrated that the surface was a uniform mix of both α-Fe_2O_3 and TiO_2 after Ar-plasma treatment. After recycle for 5 times, the corresponding amounts of O, Ti, Fe, and C were 40.2, 32.9, 22.5 and 4.4 wt%, respectively (Fig S3 **(b)**).

3.2. H_2 evolution

The photocatalytic H_2 evolution rates from different plasma treatment exposure times of heterojunction α-Fe_2O_3/TiO_2 nanocomposite are presented in Fig. 10 **(a).** α-Fe_2O_3/TiO_2 shows a photocatalytic H_2 evolution rate of 0.131 mmol h^{-1}, which suggests a fast recombination rate of photogenerated electrons and holes. After surface plasma treatment of α-Fe_2O_3/TiO_2, the H_2 evolution rates increased to 0.84, 1.25, 1.05 and 0.920 mmol h^{-1} for α-Fe_2O_3/TiO_2-5, α-Fe_2O_3/TiO_2-10, α-Fe_2O_3/TiO_2-15, and α-Fe_2O_3/TiO_2-20, respectively. We found that α-Fe_2O_3/TiO_2-10 nanocomposite showed the highest H_2 evolution rate.

The photocatalytic activities of surface plasma-treated α-Fe_2O_3/TiO_2 nanocomposite for long term H_2 evolution are presented in Fig. 10 **(b)**, the photocatalytic activity of α-Fe_2O_3/TiO_2 shows a low H_2 evolution rate. All plasma-treatment times resulted in increased photocatalytic activity of H_2 evolution compared to untreated α-Fe_2O_3/TiO_2 photocatalyst. The highest H_2 evolution rate of plasma treated samples was 5.5 $mmolh^{-1}$ for 5 h reaction time.

The performance of photocatalytic recycling stability of Ar-plasma treated α-Fe_2O_3/TiO_2 for H_2 evolution is presented in Fig. 10 **(c)**, it can be seen that after the photocatalyst recycled five times, the sample shows high stability and good performance for H_2 evolution. However, after a repeated cycling the stability slightly decreased as seen by a reduction of H_2 evolution rate. The percent stability of H_2 evolution rate was 94.27%, 93.30%, 92.18%, 90.75% and 89.32% for cycle 1, cycle 2, cycle 3, cycle 4 and cycle 5, respectively. Ibukun et al. [43] report a

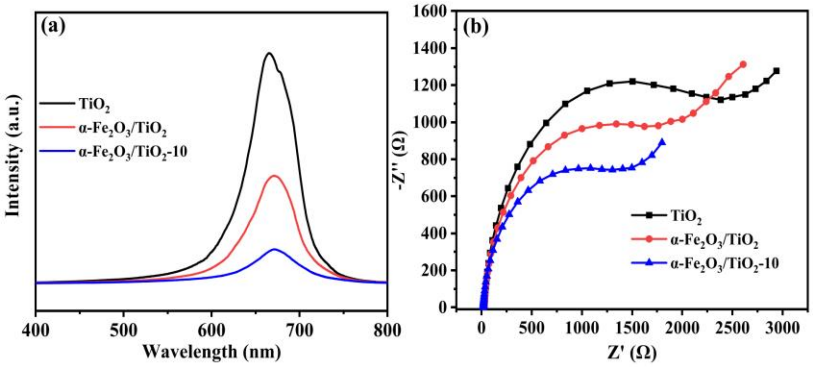

Fig. 7. (a) PL spectra of photocatalyst and (b) Nyquist plot of TiO_2, α-Fe_2O_3/TiO_2 and α-Fe_2O_3/TiO_2-10.

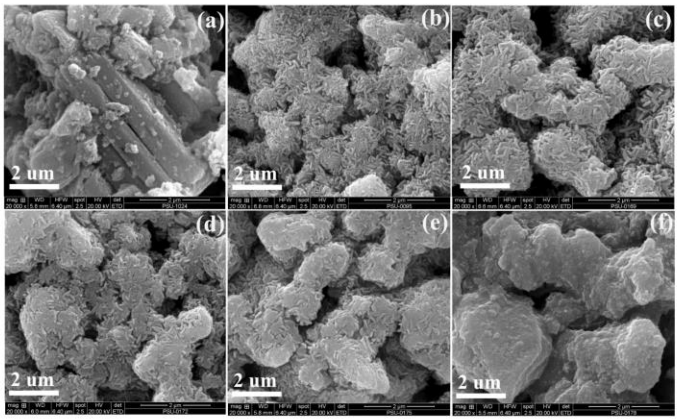

Fig. 8. SEM image of the surface of; (a) pure TiO_2, (b) α-Fe_2O_3 /TiO_2, (c) α-Fe_2O_3/TiO_2-5 (d) α-Fe_2O_3/TiO_2-10, (e) α-Fe_2O_3/TiO_2-15, and (f) α-Fe_2O_3/TiO_2-20.

similar percentage of reusability (94–96.7%) of plasma treated photocatalyst over four recycles. However, our result shows that there is no titanium detected. The iron was detected in the solution but there was not significantly difference. Statistical *t*-tests were conducted to compare the concentration of ferric ion before used and after recycle at each recycle time, the results indicate that it was not significantly of ferric ion concentration in solution after reaction at each cycle (p-value always < 0.05). Hence no leaching of ferric ion and titanium during photocatalytic reaction. It can be concluded from these results that the plasma treatment of the photocatalyst heterojunction could increase photocatalytic activity for H_2 evolution without contamination in aqueous solution during photoactivity.

The plasma treated photocatalyst exhibits a wide light response and demonstrates increased H_2 evolution rate over a longer lifetime of carrying charge. The intensity before and after recycling of the plasma treated photocatalyst was analyzed by XRD pattern, as shown in Fig. 10 **(d)**. It can be seen that after fives cycles of reaction, the XRD peaks of the α-Fe_2O_3/TiO_2 photocatalyst did not significant change. Therefore, plasma treatment improved photocatalytic activity with high efficiency, increased hydrogen evolution stability and reusability for H_2 evolution.

In addition, Table 3 presents a comparison of H_2 evolution of various photocatalyst materials that were treated with various plasma treatment methods from the literature. This shows that α-Fe_2O_3/TiO_2 has the highest H_2 evolution compared to previous reports.

The photocatalytic mechanism of H_2 evolution from water splitting for hydrogen evolution under visible light is shown in Fig. 11. Under visible light irradiation, α-Fe_2O_3/TiO_2 an electron can excite from the valence band (VB) position to the conduction band (CB) of α-Fe_2O_3 [26,39]. The excited electron can then transfer to the CB in TiO_2, because the CB band position of α-Fe_2O_3 is higher than the TiO_2 band position, and the electrons accumulate at the lower-lying CB of TiO_2 [32,34]. This causes photogenerated holes to accumulate at the VB of α-Fe_2O_3 which split a proton from a water molecule. The H^+ will react with an electron to generate a H atom and two combine to produce H_2 [27,39,69]. The photocatalytic reaction can be described by the following Eqs. (4)–(7) [27].

$$\mathrm{Ar} \rightarrow \mathrm{Ar}^+ + \mathrm{e}^- \rightarrow \alpha - \mathrm{Fe_2O_3/TiO_2} \xrightarrow{h\nu} \mathrm{TiO_2} - \mathrm{Fe_2O_3}\left(\mathrm{e}^-_{cb} + \mathrm{h}^+_{vb}\right) \quad (4)$$

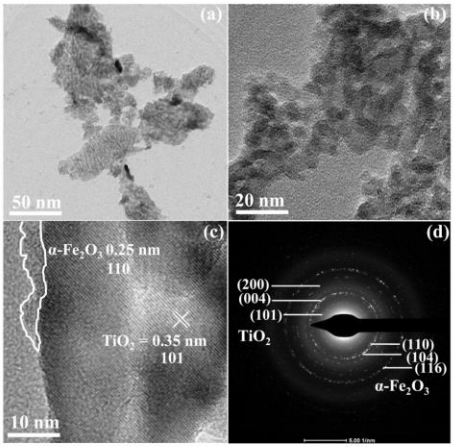

Fig. 9. TEM image of plasma treated α-Fe_2O_3/TiO_2-10 (a,b) HR-TEM (c) and (d) SAED pattern.

$$2e^-_{cb} + 2H^+ \rightarrow H^{\cdot} + H^{\cdot} \rightarrow H_2 \quad (5)$$

$$(h^+_{vb}) + H_2O \rightarrow H_2O^{+\cdot} \rightarrow {}^{\cdot}OH + H^+ \quad (6)$$

$$2\ {}^{\cdot}OH \rightarrow 2H^+ + O_2 \quad (7)$$

4. Conclusions

The photocatalytic heterojunction of α-Fe_2O_3/TiO_2 nanocomposite was successfully synthesized by the impregnation method and modified further using Ar-plasma for photocatalytic H_2 evolution.

Table 3
Comparison of plasma treatment on photocatalytic materials for H_2 evolution from the literature.

Catalyst	Plasma	Condition	H_2 evolution	Ref.
α-Fe_2O_3/TiO_2	Ar-plasma	10 min, 50 W	1250 μmol h^{-1}	This work
TiO_2/GO	Ar-plasma	30 min, 400 Pa	170 μmol h^{-1}	[45]
Pt/g-C_3N_4	Ar-Plasma	30 min, 1400 W	496.7 μmol h^{-1} g^{-1}	[47]
Ni/NiO/TiO_2	NH_3-Plasma	3–20 min, 10 kHz	1210 μmol h^{-1}	[66]
$Ti_3C_2T_x$/CdS	O_2/N_2	30 min,1400 W	825 μmol h^{-1} g^{-1}	[67]
NiO/Ta_2O_5	Ar-Plasma	30 min/NA	299 μmol h^{-1}	[68]
NiO/ZrO_2	Ar-Plasma	30 min/NA	172 μmol h^{-1}	[68]

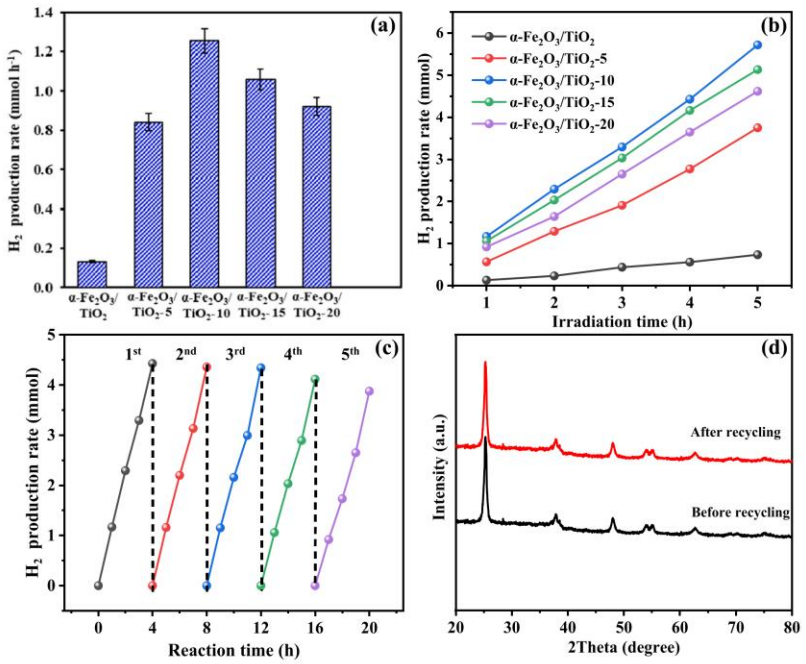

Fig. 10. Comparison of H_2 evolution rates (a) hydrogen rate of α-Fe_2O_3/TiO_2, α-Fe_2O_3/TiO_2-5, α-Fe_2O_3/TiO_2-10, α-Fe_2O_3/TiO_2-15, and α-Fe_2O_3/TiO_2-20, (b) photocatalytic long term H_2 evolution of α-Fe_2O_3/TiO_2, Fe_2O_3/TiO_2-5, α-Fe_2O_3/TiO_2-10, α-Fe_2O_3/TiO_2-15, and α-Fe_2O_3/TiO_2-20, (c) recycling long term H_2 evolution of α-Fe_2O_3/TiO_2-10 plasma and (d) XRD pattern before and after recycling.

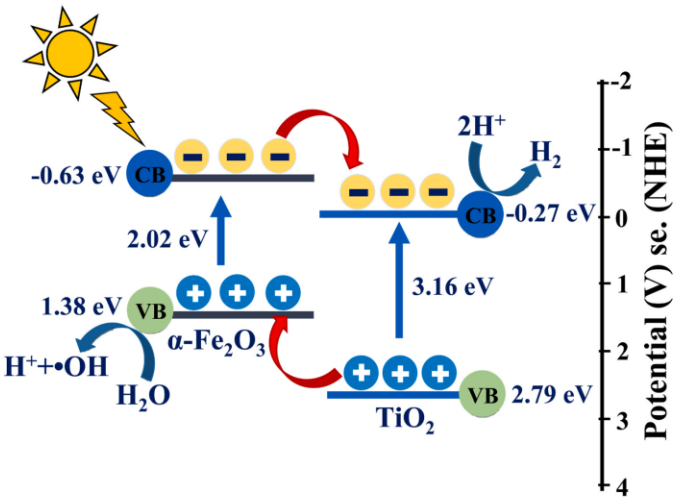

Fig. 11. Mechanism of photocatalysis over α-Fe_2O_3/TiO_2 under visible light.

- The morphology of Ar-plasma modified α-Fe_2O_3/TiO_2 nanocomposite changed from anatase TiO_2 to mixed anatase and rutile phase. The average crystallite size decreased from 23.50 to 20.13 nm and the band gap energy reduced from 1.80 to 1.93 eV.
- Ar-plasma modification of surface showed defect oxygen vacancies and Ti^{3+} in the interaction between Fe^{3+} and Ti^{4+}. The result demonstrated improved photocatalytic activity and good stability for a longer lifetime, with a reduced recombination rate of the photo-generated electron-hole pair.
- The plasma treatment time of 10 min showed the highest photocatalytic activity of H_2 evolution, which was 1.25 mmol h^{-1} for α-Fe_2O_3/TiO_2-10 nanocomposite, high efficiencies, good stability, and good reusability for H_2 evolution.

CRediT authorship contribution statement

Weerapong Bootluck: Investigation, Visualization and Original draft preparation. **Thawat Chittrakarn:** Writing - review & editing. **Kuaanan Techato:** Writing - review & editing. **Watsa Khongnakorn**: Conceptualization, Methodology, Visualization, Validation, Writing - original draft preparation, Supervision and Writing - review & editing.

Declaration of Competing Interest

The authors declare that they have no known competing financial interests or personal relationships that could have appeared to influence the work reported in this paper.

Acknowledgment

This work was supported by the Interdisciplinary Graduate School of Energy Systems (IGS-Energy), the Graduate School of Prince of Songkla University, Center of Excellent in Membrane Science and Technology, Prince of Songkla University. The authors would like to thanks Associated Prof. Dr. Yutthana Tirawanichakul for plasma equipment and Associated Prof. Dr. Warakorn Limbut for EIS analysis for the experiments.

Appendix A. Supporting information

Supplementary data associated with this article can be found in the online version at doi:10.1016/j.jece.2021.105660.

References

[1] A.A. Basheer, I. Ali, Water photo splitting for green hydrogen energy by green nanoparticles, Int. J. Hydrog. Energy 44 (2019) 11564–11573, https://doi.org/10.1016/j.ijhydene.2019.03.040.
[2] I. Dincer, C. Acar, Review and evaluation of hydrogen production methods for better sustainability, Int. J. Hydrog. Energy 40 (2014) 11094–11111, https://doi.org/10.1016/j.ijhydene.2014.12.035.
[3] C. Wang, Q. Hu, J. Huang, L. Wu, Z. Deng, Z. Liu, Y. Liu, Y. Cao, Efficient hydrogen production by photocatalytic water splitting using N-doped TiO_2 film, Appl. Surf. Sci. 283 (2013) 188–192, https://doi.org/10.1016/j.apsusc.2013.06.080.
[4] V. Kumaravel, S. Mathew, J. Bartlett, S.C. Pillai, Photocatalytic hydrogen production using metal doped TiO_2: a review of recent advances, Appl. Catal. B Environ. 244 (2019) 1021–1064, https://doi.org/10.1016/j.apcatb.2018.11.080.
[5] N.L. Reddy, V.N. Rao, M. Vijayakumar, R. Santhosh, S. Anandan, M. Karthik, M. V. Shankar, K.R. Reddy, N.P. Shetti, M.N. Nadagouda, T.M. Aminabhavi, A review on frontiers in plasmonic nano-photocatalysts for hydrogen production, Int. J. Hydrog. Energy 44 (2019) 10453–10472, https://doi.org/10.1016/j.ijhydene.2019.02.120.
[6] M. Ahmed, I. Dincer, A review on photoelectrochemical hydrogen production systems: challenges and future directions, Int. J. Hydrog. Energy 44 (2019) 2474–2507, https://doi.org/10.1016/j.ijhydene.2018.12.037.
[7] C. Acar, I. Dincer, A review and evaluation of photoelectrode coating materials and methods for photoelectrochemical hydrogen production, Int. J. Hydrog. Energy 41 (2016) 7950–7959, https://doi.org/10.1016/j.ijhydene.2015.11.160.
[8] Q. Wei, Y. Yang, H. Liu, J. Hou, M. Liu, F. Cao, L. Zhao, Experimental study on direct solar photocatalytic water splitting for hydrogen production using surface uniform concentrators, Int. J. Hydrog. Energy 43 (2018) 13745–13753, https://doi.org/10.1016/j.ijhydene.2018.01.135.
[9] A.M.M.I. Qureshy, M. Ahmed, I. Dincer, Performance assessment study of photo-electro-chemical water-splitting reactor designs for hydrogen production, Int. J. Hydrog. Energy 44 (2019) 9237–9247, https://doi.org/10.1016/j.ijhydene.2019.01.280.
[10] M.Y. Azwar, M.A. Hussain, A.K. Abdul-wahab, Development of biohydrogen production by photobiological, fermentation and electrochemical processes: a review, Renew. Sustain. Energy Rev. 31 (2014) 158–173, https://doi.org/10.1016/j.rser.2013.11.022.
[11] C.-W. Huang, B.-S. Nguyen, J.C.-S. Wu, V.-H. Nguyen, A current perspective for photocatalysis towards the hydrogen production from biomass-derived organic substances and water, Int. J. Hydrog. Energy (2019), https://doi.org/10.1016/j.ijhydene.2019.08.121.

[12] R. Fiorenza, S. Sciré, L. D'Urso, G. Compagnini, M. Bellardita, L. Palmisano, Efficient H_2 production by photocatalytic water splitting under UV or solar light over variously modified TiO_2-based catalysts, Int. J. Hydrog. Energy 44 (2019) 14796–14807, https://doi.org/10.1016/j.ijhydene.2019.04.035.
[13] A. Fujishima, T.N. Rao, D.A. Tryk, Titanium dioxide photocatalysis, J. Photochem. Photobiol. C Photochem. Rev. 1 (2000) 1–21, https://doi.org/10.1016/S1389-5567(00)00002-2.
[14] H. Wang, L. Zhang, Z. Chen, J. Hu, S. Li, Z. Wang, J. Liu, X. Wang, Semiconductor heterojunction photocatalysts: design, construction, and photocatalytic performances, Chem. Soc. Rev. 43 (2014) 5234–5244, https://doi.org/10.1039/c4cs00126e.
[15] X. Zhang, Y. Xie, H. Chen, J. Guo, A. Meng, C. Li, One-dimensional mesoporous Fe_2O_3@TiO_2 core – shell nanocomposites: rational design, synthesis and application as high-performance photocatalyst in visible and uv light region, Appl. Surf. Sci. 317 (2014) 43–48, https://doi.org/10.1016/j.apsusc.2014.08.099.
[16] M. Kanna, S. Wongnawa, Mixed amorphous and nanocrystalline TiO_2 powders prepared by sol-gel method: characterization and photocatalytic study, Mater. Chem. Phys. 110 (2008) 166–175, https://doi.org/10.1016/j.matchemphys.2008.01.037.
[17] H.R. Khaledian, P. Zolfaghari, V. Elhami, M. Aghbolaghy, S. Khorram, A. Karimi, A. Khataee, Modification of immobilized titanium dioxide nanostructures by argon plasma for photocatalytic removal of organic dyes, Molecules (2019) 1–19, https://doi.org/10.3390/molecules24030383.
[18] K. Wen, M. Liu, X. Liu, C. Deng, K. Zhou, Deposition of photocatalytic TiO_2 coating by modifying the solidification pathway in plasma spraying, Coatings 7 (2017) 1–9, https://doi.org/10.3390/coatings7100169.
[19] Y. Xu, Y. Zhang, T. He, K. Ding, X. Huang, H. Li, J. Shi, Y. Guo, J. Zhang, The effects of thermal and atmospheric pressure radio frequency plasma annealing in the crystallization of TiO_2 thin films, Coatings 9 (2019) 1–10, https://doi.org/10.3390/coatings9060357.
[20] X. Zhang, L. Zhang, Y. Li, L. Di, Atmospheric-pressure cold plasma for fabrication of anatase–rutile mixed TiO_2 with the assistance of ionic liquid, Catal. Today 256 (2015) 215–220, https://doi.org/10.1016/j.cattod.2015.04.033.
[21] B.M. Pirzada, O. Mehraj, S.A. Bhat, S. Sabir, Efficient visible-light-driven photocatalytic activity and enhanced charge transfer properties over Mo-doped WO_3/TiO_2 nanocomposites, J. Environ. Chem. Eng. 6 (2018) 3204–3212, https://doi.org/10.1016/j.jece.2018.05.004.
[22] E. Baran Aydın, G. Sığırcık, Preparations of different ZnO nanostructures on TiO_2 nanotube via electrochemical method and its application in hydrogen production, Int. J. Hydrog. Energy 44 (2019) 11488–11502, https://doi.org/10.1016/j.ijhydene.2019.03.123.
[23] S.S. Lee, H. Bai, Z. Liu, D.D. Sun, Electrospun TiO_2/SnO_2 nanofibers with innovative structure and chemical properties for highly efficient photocatalytic H_2 generation, Int. J. Hydrog. Energy 37 (2012) 10575–10584, https://doi.org/10.1016/j.ijhydene.2012.04.098.
[24] L. Yan, F. Yang, C.Y. Tao, X. Luo, L. Zhang, Highly efficient and stable Cu_2O–TiO_2 intermediate photocatalytic water splitting, Ceram. Int. 46 (2020) 9455–9463, https://doi.org/10.1016/j.ceramint.2019.12.206.
[25] O.F.S. Khasawneh, P. Palaniandy, P. Palaniandy, M. Ahmadipour, H. Mohammadi, M.R. Bin Hamdan, Removal of acetaminophen using Fe_2O_3-TiO_2 nanocomposites by photocatalysis under simulated solar irradiation: optimization study, J. Environ. Chem. Eng. 9 (2021), 104921, https://doi.org/10.1016/j.jece.2020.104921.
[26] X. Li, H. Lin, X. Chen, H. Niu, J. Liu, T. Zhang, F. Qu, Dendritic α-Fe_2O_3/TiO_2 nanocomposites with improved visible light photocatalytic activity, Phys. Chem. Chem. Phys. 18 (2016) 9176–9185, https://doi.org/10.1039/c5cp06681f.
[27] A. Madhumitha, V. Preethi, S. Kanmani, Photocatalytic hydrogen production using TiO_2 coated iron-oxide core shell particles, Int. J. Hydrog. Energy 43 (2018) 3946–3956, https://doi.org/10.1016/j.ijhydene.2017.12.127.
[28] X. Li, H. Lin, X. Chen, H. Niu, J. Liu, T. Zhang, F. Qu, Peripheral lymphoid volume expansion and maintenance are controlled by gut microbiota via RALDH+ dendritic cells, Immunity 44 (2016) 330–342, https://doi.org/10.1039/C5CP06681F.
[29] M.H.H. Mahmoud, A.A. Ismail, M.M.S. Sanad, Developing a cost-effective synthesis of active iron oxide doped titania photocatalysts loaded with palladium, platinum or silver nanoparticles, Chem. Eng. J. 187 (2012) 96–103, https://doi.org/10.1016/j.cej.2012.01.105.
[30] M. Mishra, D.M. Chun, α-Fe_2O_3 as a photocatalytic material: a review, Appl. Catal. A Gen. 498 (2015) 126–141, https://doi.org/10.1016/j.apcata.2015.03.023.
[31] H. Fu, S. Sun, X. Yang, W. Li, X. An, H. Zhang, Y. Dong, X. Jiang, A. Yu, A facile coating method to construct uniform porous α-Fe_2O_3@TiO_2 core-shell nanostructures with enhanced solar light photocatalytic activity, Powder Technol. 328 (2018) 389–396, https://doi.org/10.1016/j.powtec.2018.01.067.
[32] R.M. Mohamed, M.W. Kadi, A.A. Ismail, A Facile synthesis of mesoporous α-Fe_2O_3/TiO_2 nanocomposites for hydrogen evolution under visible light, Ceram. Int. 46 (2020) 15604–15612, https://doi.org/10.1016/j.ceramint.2020.03.107.
[33] H. Lu, S. Fang, J. Hu, B. Chen, R. Zhao, H. Li, C.M. Li, J. Ye, Fabrication of a TiO_2/Fe_2O_3 core/shell nanostructure by pulse laser deposition toward stable and visible light photoelectrochemical water splitting, ACS Omega 5 (2020) 19861–19867, https://doi.org/10.1021/acsomega.0c02838.
[34] S. Zhu, F. Yao, C. Yin, Y. Li, W. Peng, J. Ma, D. Zhang, Fe_2O_3/TiO_2 photocatalyst of hierarchical structure for H_2 production from water under visible light irradiation, Microporous Mesoporous Mater. 190 (2014) 10–16, https://doi.org/10.1016/j.micromeso.2014.01.018.
[35] G.L. Chiarello, M.V. Dozzi, E. Selli, TiO_2-based materials for photocatalytic hydrogen production, J. Energy Chem. 26 (2017) 250–258, https://doi.org/10.1016/j.jechem.2017.02.005.
[36] A. Meng, L. Zhang, B. Cheng, J. Yu, Dual cocatalysts in TiO_2 photocatalysis, Adv. Mater. 1807660 (2019) 1–31, https://doi.org/10.1002/adma.201807660.
[37] S.J.A. Moniz, S.A. Shevlin, X. An, Z.X. Guo, J. Tang, Fe_2O_3-TiO_2 nanocomposites for enhanced charge separation and photocatalytic activity, Chem. A Eur. J. 20 (2014) 15571–15579, https://doi.org/10.1002/chem.201403489.
[38] J. Krysa, M. Zlamal, S. Kment, M. Brunclikova, Z. Hubicka, TiO_2 and Fe_2O_3 films for photoelectrochemical water splitting, Molecules 20 (2015) 1046–1058, https://doi.org/10.3390/molecules20011046.
[39] R. Huang, R. Liang, H. Fan, S. Ying, L. Wu, X. Wang, G. Yan, Enhanced photocatalytic fuel denitrification over TiO_2/α-Fe_2O_3 nanocomposites under visible light irradiation, Sci. Rep. 7 (2017) 1–10, https://doi.org/10.1038/s41598-017-08439-3.
[40] Y. Li, W. Wang, F. Wang, L. Di, S. Yang, S. Zhu, Y. Yao, C. Ma, B. Dai, F. Yu, Enhanced photocatalytic degradation of organic dyes via defect-rich TiO_2 prepared by dielectric barrier discharge plasma, Nanomaterials 9 (2019), https://doi.org/10.3390/nano9050720.
[41] G.D. Rajmohan, X.J. Dai, T. Tsuzuki, P.R. Lamb, J. Du Plessis, F. Huang, Y. B. Cheng, Modifying TiO_2 surface architecture by oxygen plasma to increase dye sensitized solar cell efficiency, Thin Solid Films 545 (2013) 521–526, https://doi.org/10.1016/j.tsf.2013.07.072.
[42] M.R. Mohammadizadeh, M. Bagheri, S. Aghabagheri, Y. Abdi, Photocatalytic activity of TiO_2 thin films by hydrogen DC plasma, Appl. Surf. Sci. 350 (2015) 43–49, https://doi.org/10.1016/j.apsusc.2015.03.196.
[43] O. Ibukun, H.K. Jeong, Improved photocatalytic efficiency of titanium dioxide-hematite composite by air plasma, Chem. Phys. Lett. 730 (2019) 259–265, https://doi.org/10.1016/j.cplett.2019.06.022.
[44] J. Horlyck, A. Nashira, E. Lovell, R. Daiyan, N. Bedford, Y. Wei, R. Amal, J. Scott, Plasma treating mixed metal oxides to improve oxidative performance via defect generation, Materials 12 (2019) 2756, https://doi.org/10.3390/ma12172756.
[45] X. Kong, H. Huang, Z. Li, Y. Liang, Z. Li, S. Zhu, Facile synthesis of defected TiO_2-x (B) nanosheet/graphene oxide hybrids with high photocatalytic H_2 activity, J. Mater. Sci. Technol. 80 (2021) 171–178, https://doi.org/10.1016/j.jmst.2021.01.005.
[46] X. Kong, Y. Xu, Z. Cui, Z. Li, Y. Liang, Z. Gao, S. Zhu, X. Yang, Defect enhances photocatalytic activity of ultrathin TiO_2 (B) nanosheets for hydrogen production by plasma engraving method, Appl. Catal. B Environ. 230 (2018) 11–17, https://doi.org/10.1016/j.apcatb.2018.02.019.
[47] Q. Xiang, F. Li, D. Zhang, Y. Liao, H. Zhou, Plasma-based surface modification of g-C_3N_4 nanosheets for highly efficient photocatalytic hydrogen evolution, Appl. Surf. Sci. 495 (2019), 143520, https://doi.org/10.1016/j.apsusc.2019.07.262.
[48] D. Sun, Y. Han, S. Gao, X. Zhang, Surface modification of titania-coated cobalt ferrite magnetic photocatalyst by cold plasma, Surf. Coat. Technol. 228 (2013) S516–S519, https://doi.org/10.1016/j.surfcoat.2012.04.072.
[49] R. Kawakami, K. Tominaga, K. Okada, T. Nouda, T. Inaoka, A. Takeichi, T. Fukudome, K. Murao, Etch damage characteristics of TiO_2 thin films by capacitively coupled RF Ar plasmas, Vacuum 84 (2010) 1393–1397, https://doi.org/10.1016/j.vacuum.2010.01.006.
[50] M. Benčina, I. Junkar, R. Zaplotnik, M. Valant, A. Iglič, M. Mozetič, Plasma-induced crystallization of TiO_2 nanotubes, Materials 12 (2019), https://doi.org/10.3390/ma12040626.
[51] L. Peng, T. Xie, Y. Lu, H. Fan, D. Wang, Synthesis, photoelectric properties and photocatalytic activity of the Fe_2O_3/TiO_2 heterogeneous photocatalysts, Phys. Chem. Chem. Phys. 12 (2010) 8033–8041, https://doi.org/10.1039/c002460k.
[52] W. Khongnakorn, W. Bootluck, P. Jutaporn, Surface modification of FO membrane by plasma-grafting polymerization to minimize protein fouling, J. Water Process Eng. 38 (2020), 101633, https://doi.org/10.1016/j.jwpe.2020.101633.
[53] J. Saichanapan, K. Promsuwan, W. Limbut, Adsorption and determination of sibutramine in illegal slimming product using porous graphene ink-modified electrode, Talanta 212 (2020), 120788, https://doi.org/10.1016/j.talanta.2020.120788.
[54] Z. Haider, Y.S. Kang, Facile preparation of hierarchical TiO_2 nano structures: Growth mechanism and enhanced photocatalytic H_2 production from water splitting using methanol as a sacrificial reagent, ACS Appl. Mater. Interfaces 6 (2014) 10342–10352, https://doi.org/10.1021/am501796m.
[55] Q. Jiang, L. Li, J. Bi, S. Liang, M. Liu, Design and synthesis of TiO_2 hollow spheres with spatially separated dual cocatalysts for efficient photocatalytic hydrogen production, Nanomaterials 7 (2017) 24, https://doi.org/10.3390/nano7020024.
[56] D. Yu, L. Li, M. Wu, J.C. Crittenden, Enhanced photocatalytic ozonation of organic pollutants using an iron-based metal-organic framework, Appl. Catal. B Environ. 251 (2019) 66–75, https://doi.org/10.1016/j.apcatb.2019.03.050.
[57] S. Topcu, G. Jodhani, P.I. Gouma, Optimized nanostructured TiO_2 photocatalysts, Front. Mater. 3 (2016) 1–9, https://doi.org/10.3389/fmats.2016.00035.
[58] B. Wang, C. Li, H. Cui, J. Zhang, J. Zhai, Q. Li, Fabrication and enhanced visible-light photocatalytic activity of Pt-deposited TiO_2 hollow nanospheres, Chem. Eng. J. 223 (2013) 592–603, https://doi.org/10.1016/j.cej.2013.03.052.
[59] S. Zhu, F. Yao, C. Yin, Y. Li, W. Peng, J. Ma, D. Zhang, Fe_2O_3/TiO_2 photocatalyst of hierarchical structure for H_2 production from water under visible light irradiation, Microporous Mesoporous Mater. 190 (2014) 10–16, https://doi.org/10.1016/j.micromeso.2014.01.018.
[60] Y.P. Bhoi, F. Fang, X. Zhou, Y. Li, X. Sun, J. Wang, W. Huang, Single step combustion synthesis of novel Fe_2TiO_5/α-Fe_2O_3/TiO_2 ternary photocatalyst with combined double type-II cascade charge migration processes and efficient photocatalytic activity, Appl. Surf. Sci. 525 (2020), 146571, https://doi.org/10.1016/j.apsusc.2020.146571.
[61] A. Naldoni, M. Allieta, S. Santangelo, M. Marelli, F. Fabbri, S. Cappelli, C. L. Bianchi, R. Psaro, V. Dal Santo, Effect of nature and location of defects on

bandgap narrowing in black TiO_2 nanoparticles, J. Am. Chem. Soc. 134 (2012) 7600–7603, https://doi.org/10.1021/ja3012676.

[62] X. Fang, G. Lu, A. Mahmood, Z. Tang, Z. Liu, L. Zhang, Y. Wang, J. Sun, A novel ternary Mica/TiO_2/Fe_2O_3 composite pearlescent pigment for the photocatalytic degradation of acetaldehyde, J. Photochem. Photobiol. A Chem. 400 (2020), 112617, https://doi.org/10.1016/j.jphotochem.2020.112617.

[63] H. Zhao, J. Kang, H. Nan, G. Yang, H. Wei, H. Chen, G. Wang, H. Lin, Preparation and enhanced UV–Visible light photoelectrocatalytic activity of TiO_2 -Fe_2O_3/Cu ternary nanocomposites, ChemistrySelect 4 (2019) 2892–2897, https://doi.org/10.1002/slct.201803345.

[64] L. Sirghi, Y. Hatanaka, K. Sakaguchi, Photocatalytic property of titanium dioxide thin films deposited by radio frequency magnetron sputtering in argon and water vapour plasma, Appl. Surf. Sci. 352 (2015) 38–41, https://doi.org/10.1016/j.apsusc.2015.04.157.

[65] J. Liu, S. Yang, W. Wu, Q. Tian, S. Cui, Z. Dai, F. Ren, X. Xiao, C. Jiang, 3D flowerlike α-Fe_2O_3@TiO_2 core-shell nanostructures: general synthesis and enhanced photocatalytic performance, ACS Sustain. Chem. Eng. 3 (2015) 2975–2984, https://doi.org/10.1021/acssuschemeng.5b00956.

[66] S. Hu, F. Li, Z. Fan, J. Gui, Improved photocatalytic hydrogen production property over Ni/NiO/N-TiO_{2-x} heterojunction nanocomposite prepared by NH_3 plasma treatment, J. Power Sour. 250 (2014) 30–39, https://doi.org/10.1016/j.jpowsour.2013.10.132.

[67] Q.X. Yali Yang, Dainan Zhang, Plasma-modified $Ti_3C_2T_x$/CdS hybrids with oxygen-containing groups for high-efficiency photocatalytic hydrogen production, Nanoscale 11 (2019) 18797–18805, https://doi.org/10.1039/b000000x.

[68] J.J. Zou, C.J. Liu, Y.P. Zhang, Control of the metal-support interface of NiO-loaded photocatalysts via cold plasma treatment, Langmuir 22 (2006) 2334–2339, https://doi.org/10.1021/la052135u.

[69] G. Carraro, A. Gasparotto, C. Maccato, E. Bontempi, D. Barreca, Fe_2O_3-TiO_2 nanocomposites on activated carbon fibers by a plasma-assisted approach, Surf. Coat. Technol. 307 (2016) 352–358, https://doi.org/10.1016/j.surfcoat.2016.08.050.

CHAPTER 4
CONCLUSIONS

In summary, the development of photocatalytic material of improving photocatalytic activity by noble metal deposition and plasma treatment for hydrogen production. The photocatalyst heterojunction of S-scheme α-Fe_2O_3/TiO_2 nanocomposite with the ternary of Pd were synthesis by sol-gel methods for increased H_2 production rate. As the result of the characterization, the average crystallite size was 22 nm. The band gap energy was decreased from 2.18 to 2.00 eV and the stronger intensity absorption under visible light. The deposition of Pd ternary over α-Fe_2O_3/TiO_2 was improve the recombination and separation efficiency of charge carriers. The H_2 evolution rate was increased from 74.60 μmol h^{-1} to 349.54 μmol h^{-1} and the reusability was decreased 10 % under visible light. The possible mechanism of heterojunction photocatalytic has been presented in S-Scheme heterojunction and Type-II heterojunction has been descript in Chapter 2 and Chapter 3.

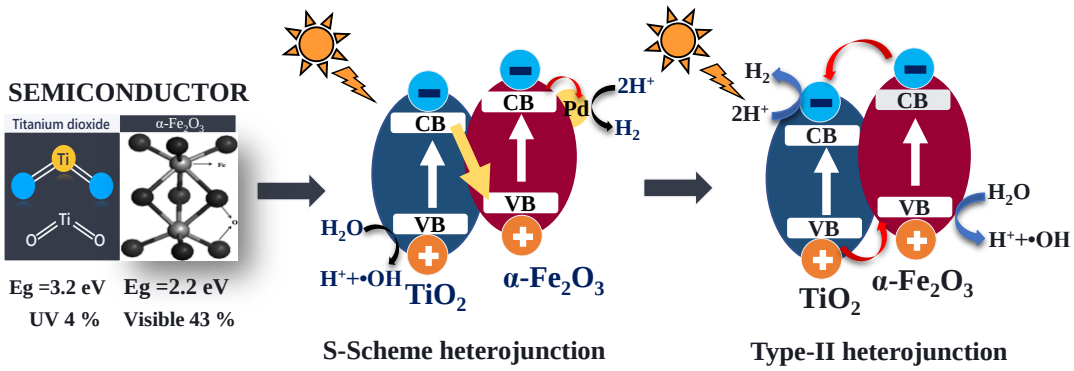

Fig. 4.1 Mechanism of photocatalyst over α-Fe_2O_3/TiO_2 and Pd cocatalyst in S-Scheme and Type-II heterojunction

Table 4.1 Summarize of characterization and performance of photocatalyst samples

Photocatalyst	UV-vis (λ,nm)	Average crystallite size (nm)	Crystallinity (%)	Band gap Energy (eV)	H_2 production (μmol h^{-1})	Reusability
α-Fe_2O_3/TiO_2	≥420	23.5	92.55	2.18	74.60	NA
α-Fe_2O_3/TiO_2-Pd	≥420	22.11	94.54	2.00	349.54	90%
α-Fe_2O_3/TiO_2-10	≥420	21.50	78.23	1.84	1250	94%

The modification of photocatalytic heterojunction α-Fe_2O_3/TiO_2 by Ar plasma at 50 watts of 5-20 min was investigated. As a result, the plasma modification was obtained mixed of anatase and rutile phase were presented, the average crystal size was decreased from 25 nm to 20 nm and the band gap energy was reduced from 2.18 eV to 1.84 eV. The charge transfer resistance was reduced from 2.24 to 1.90 kΩ for α-Fe_2O_3/TiO_2 and α-Fe_2O_3/TiO_2-10. The Ar plasma treatment at 10 min (α-Fe_2O_3/TiO_2-10) shows the highest H_2 production rate at 1250 μmol h^{-1} when compare with the α-Fe_2O_3/TiO_2. Therefore, the concludes in this work to the development of α-Fe_2O_3/TiO_2 photocatalyst of characterization and the performance is summarized in Table 4.1 Chapter 4.

APPENDIX

PAPER I SUPPORTING INFORMATION

Supporting Information

S-scheme α-Fe_2O_3/TiO_2 photocatalyst with Pd cocatalyst for enhanced photocatalytic H_2 production activity and stability

Weerapong Bootluck[a,b], Thawat Chittrakarn[b], Kuaanan Techato[a,c], Panitan Jutaporn[d], Watsa Khongnakorn[b,e,*]

[a]Faculty of Environmental Management, Prince of Songkla University, Hat Yai, Songkhla, 90112, Thailand.

[b]Center of Excellence in Membrane Science and Technology, Prince of Songkla University, Hat Yai, Songkhla, 90112, Thailand.

[c]PSU Energy Systems Research Institute, Prince of Songkla University, Hat Yai, Songkhla, 90112, Thailand.

[d]Research Center for Environmental and Hazardous Substance Management (EHSM), Department of Environmental Engineering, Faculty of Engineering, Khon Kaen University, Khon Kaen 40002, Thailand.

[e]Department of Civil and Environmental Engineering, Faculty of Engineering, Prince of Songkla University, Hat Yai, Songkhla, 90112, Thailand.

**Corresponding Author: watsa.k@psu.ac.th*

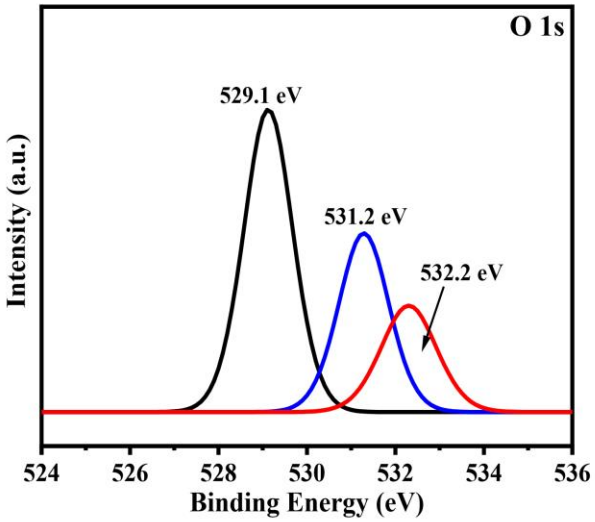

Fig. S1: XPS of O 1s spectra of α- Fe_2O_3/TiO_2-Pd

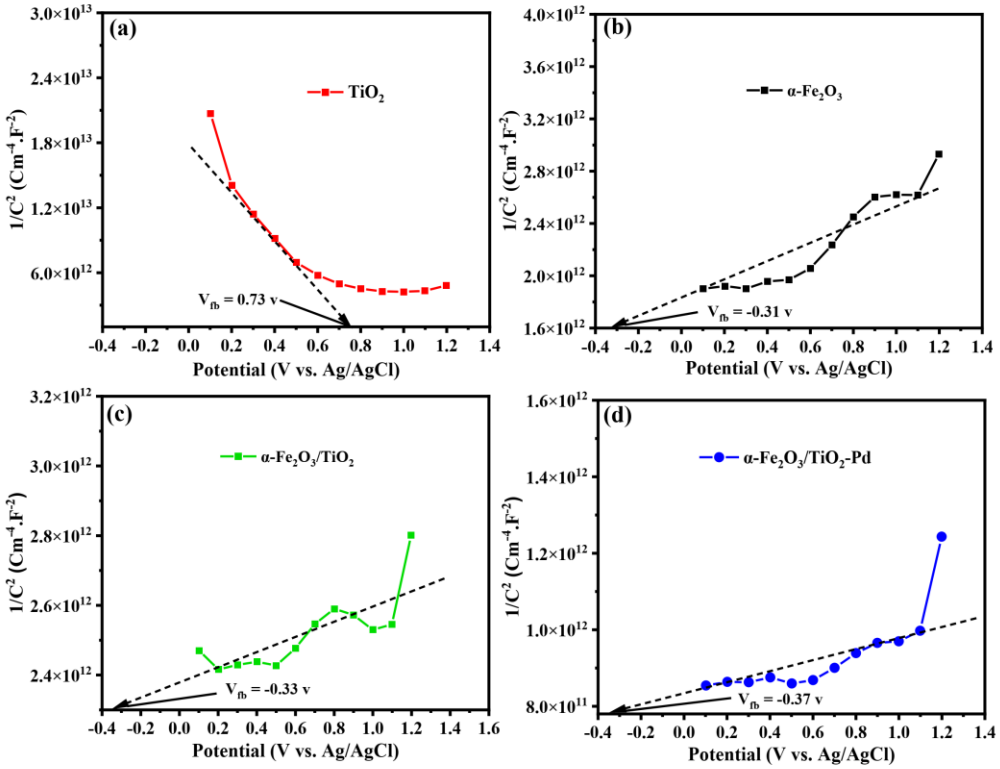

Fig. S2: Mott Schottky plot for TiO_2, α-Fe_2O_3, α-Fe_2O_3/TiO_2 and α-Fe_2O_3/TiO_2-Pd

PAPER II SUPPORTING INFORMATION

Supporting Information

Modification of surface α-Fe_2O_3/TiO_2 photocatalyst nanocomposite with enhanced photocatalytic activity by Ar gas plasma treatment for hydrogen evolution

Weerapong Bootluck[1,2], Thawat Chittrakarn[2], Kuaanan Teachato[1,3] and Watsa Khongnakorn[2,4*]

[1]Faculty of Environmental Management, Prince of Songkla University, Hat Yai, Songkhla 90112, Thailand.
[2]Center of Excellence in Membrane Science and Technology, Prince of Songkla University, Hat Yai, Songkhla 90112, Thailand.
[3]PSU Energy Systems Research Institute, Prince of Songkla University, Hat Yai, Songkhla 90112, Thailand
[4]Department of Civil and Environmental Engineering, Faculty of Engineering, Prince of Songkla University, Hat Yai, Songkhla 90112, Thailand.

*Corresponding author: *watsa.k@psu.ac.th*

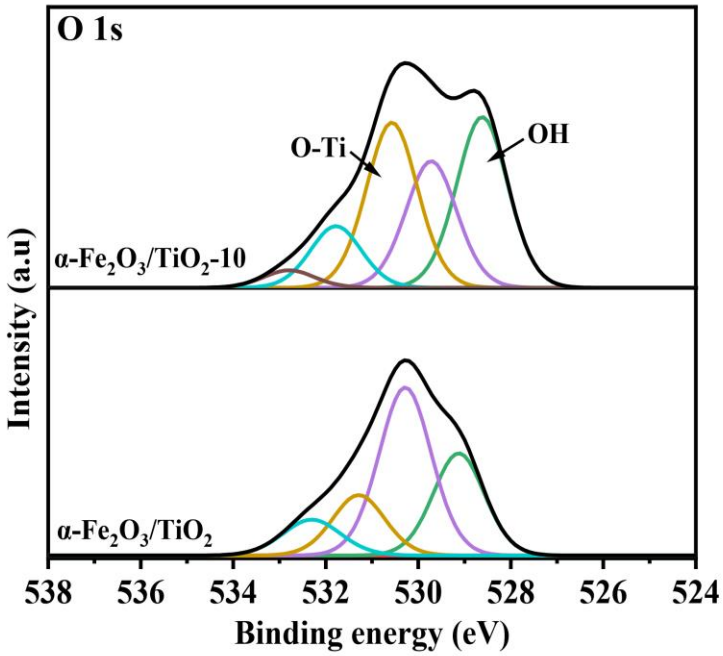

Fig. S1. XPS pattern of O1s α-Fe_2O_3/TiO_2 and α-Fe_2O_3/TiO_2-10.

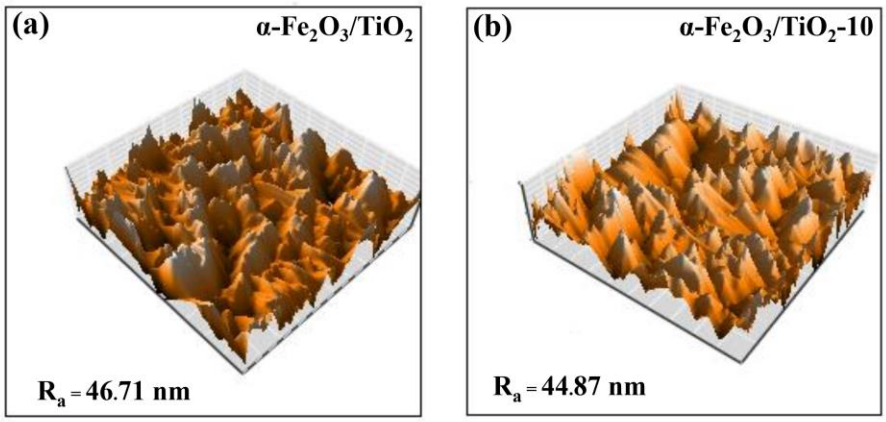

Fig. S2. AFM of (a) α-Fe_2O_3/TiO_2 and (b) α-Fe_2O_3/TiO_2-10.

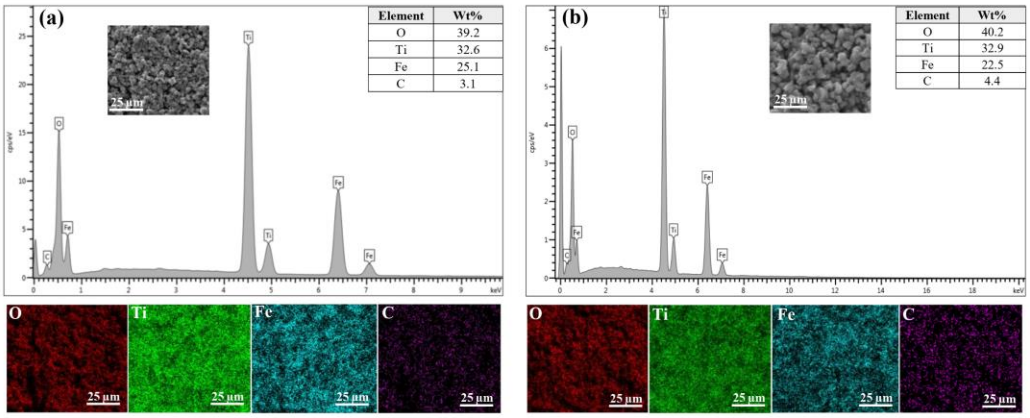

Fig. S3. EDS mapping spectrum of α-Fe_2O_3/TiO_2-10, (a) before used and (b) after used 5 times.

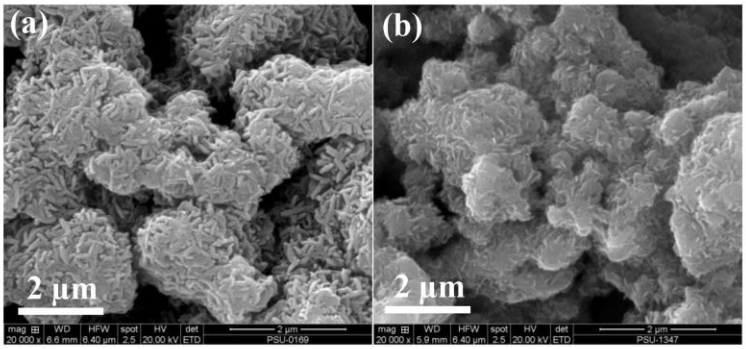

Fig. S4. SEM image of α-Fe_2O_3/TiO_2-10, (a) before used and (b) after used 5 times.

VITAE

Name Mr. Weerapong Bootluck

Student ID 5910930033

Education Attainment

Degree	Name of Institution	Year of Graduate
Bachelors of Science (Chemistry-Biology)	Prince of Songkla University	2010
Master of Science (Environmental Management)	Prince of Songkla University	2015

Awards

- Ph.D. Scholarship from Interdisciplinary Graduate School of Energy System (IGS-Energy), Prince of Songkla University
- The research grant from Graduate School, Prince of Songkla University
- The scholarship from the Center of Excellence in Membrane science and Technology, Prince of Songkla University

Publication

- **Bootluck, W**., Chittrakarn, T., Techato, K., Jutaporn, P and Khongnakorn, W. 2021. S-Scheme α-Fe_2O_3/TiO_2 Photocatalyst with Pd Cocatalyst for Enhanced Photocatalytic H_2 Production Activity and Stability. Catalysis Letters, 1-17.
- **Bootluck, W**., Chittrakarn, T., Techato, K., and Khongnakorn, W. 2021. Modification of surface α-Fe_2O_3/TiO_2 photocatalyst nanocomposite with enhanced photocatalytic activity by Ar gas plasma treatment for hydrogen evolution. Journal of Environmental Chemical Engineering, 9 (4), 105660.

International Conference

- **Weerapong Bootluck**, Thawat Chittrakarn, Kuaanan Techato, Watsa Khongnakorn. Modification of surface α-Fe_2O_3/TiO_2 photocatalyst nanocomposite with enhanced photocatalytic activity by Ar gas plasma treatment for hydrogen evolution. Regional Congress on Membrane Technology 2020 (RCOM 2020) and Regional Conference on Environmental Engineering (RCEnvE 2020). January 16-17 Johor, Malaysia, 16-17, 2021
- **W. Bootluck**, N. Junchoob, N. Meesiang, W. Khongnakorn and T. Chittrakarn. Dye Sensitizer of Chlorophyll Mixed with TiO_2 nanoparticle in photocatalytic for enhancing the hydrogen production. International Conference on Membrane Science and Technology (MST2019). Nanyang Technology University, Singapore, June 13-14, 2019
- **Weerapong Bootluck**, Watsa Khongnakorn, Thawat Chittrakarn. Modification of photocatalytic membrane for hydrogen separation by plasma gas. International Conference on Sustainable Energy Management for Climate Change Adaptation and Mitigation. August 17, 2017, Hat Yai, Songkla, Thailand